Department of Pathology

CHAMP

Clinical, Hemato-, Anatomic, Molecular Pathology

Research Day

Feb. 8, 2018

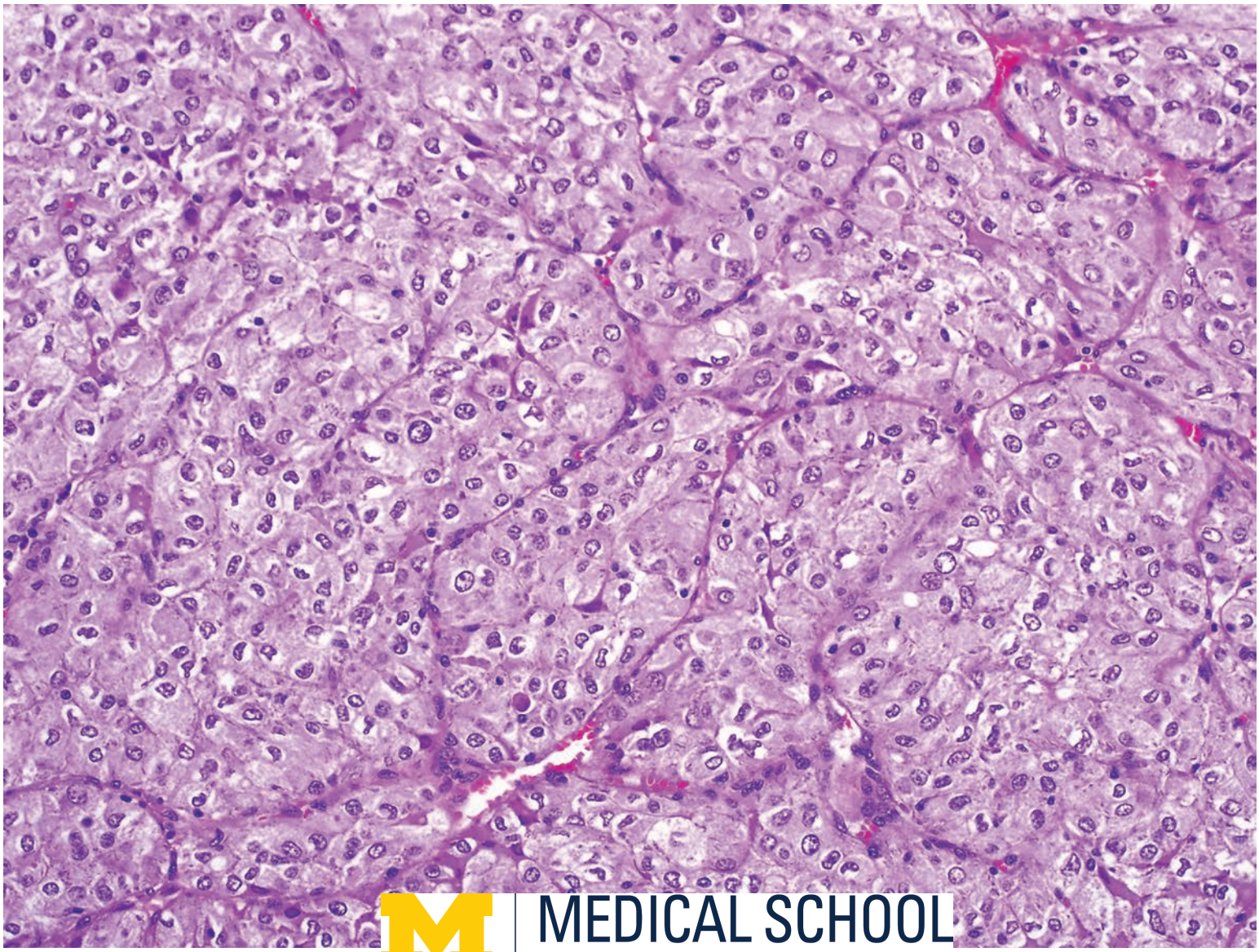

MEDICAL SCHOOL
UNIVERSITY OF MICHIGAN

Welcome

9th Annual

CHAMP

Clinical, Hemato-, Anatomic, Molecular Pathology Research Day

Thursday, February 8, 2018

Towsley Lobby and Dow Auditorium,
University of Michigan Hospital

Learning Objectives: Attendees will learn new tools and techniques to apply to their own areas of investigative interest. In addition, they will identify opportunities for collaborative research. The success of this conference will be measured in an increased number of research projects, presentations at national and international meetings, and peer-reviewed publications.

Target Audience: University of Michigan Pathology Faculty and Trainees

Conference Directors:

David R. Lucas, MD
A. James French Professor of Anatomic Pathology
Director, Division of Anatomic Pathology
Department of Pathology
Michigan Medicine

Thomas, J. Giordano, MD PhD
Henry Clay Bryant Professor of Pathology
Director, Tissue and Molecular Pathology Core
Director, GI Spore Biosample Core
Director, Molecular Pathology
Compliance Officer
Department of Pathology
Michigan Medicine

David F. Keren, MD
Professor of Pathology
Director, Division of Clinical Pathology
Department of Pathology
Michigan Medicine

Aaron M. Udager, MD, PhD
Clinical Assistant Professor
Anatomic Pathology
Department of Pathology
Michigan Medicine

Table of Contents

#28 - Retrospective Analysis of Follicular Neoplasm Cytomorphology Using a Robust and Semi-automated Digital Image Algorithm 27
Keluo Yao, Xin Jing, Amer Heider, Judy C Pang, Robertson Davenport, Madelyn Lew

#29 - Targeted Genomic Profiling Reveals Highly Recurrent Molecular Alterations in the Malignant Progression of Sinonasal Papilloma to Sinonasal Squamous Cell Carcinoma, including CDKN2A Mutation/Deletion and TP53 Mutation 28
Osman H. Yilmaz, Komal R. Kunder, Jonathan B. McHugh, Bryan L. Betz, Scott A. Tomlins, Noah A. Brown, Aaron M. Udager

#30 - High Rate of FISH False Negative Results in the Detection of Homozygous Loss of CDKN2A in Difficult Melanocytic Tumors 28
Nicholas Zoumberos, Kenneth Yu, Min Wang, Paul Harms, May Chan, Rajiv Patel, Lori Lowe, Douglas Fullen, Aleodor Andea

6:30 - 7:15 pm - KEYNOTE SPEAKER: **Dr. Pedram Argani** 29
Breast Pathology Director
Professor of Pathology and Oncology
Department of Pathology
Johns Hopkins Hospital

"MiT Family Translocation Carcinomas of the Kidney"

CHAMP
Program Schedule
9th Annual

Clinical, Hemato-, Anatomic, Molecular Pathology
Research Day
Thursday, February 8, 2018

3:00-4:30pm **PLATFORM SESSION** (Moderators: Drs. Paul Harms and Sarah Choi)
3:00pm Welcome and Introduction (Dr. Aaron Udager)

3:05pm **GIESEN LECTURE AWARDEE -**
Giesen Lecture: Dr. Emily McMullen
"Metaplastic Breast Carcinomas Exhibit Low CCN6 Expression with Activation of the IG F2BP2-HMGA2-Signaling Axis"

3:30pm **Dr. Ulysses Balis**
"A Generalizable Deep Learning Model for Extraction of Diagnostic Data from Histopathological Data Sets"

3:45pm **Dr. Andi Cani**
"Development of a Whole Urine, Next-Generation Sequencing-Based Assay for Early Detection of Aggressive Prostate Cancer"

4:00pm **Dr. Steven Burke Van Norman**
"Cytogenomic Array Detects a High-Risk Subset of Myelodysplastic Syndrome Invisible to Conventional Karyotype"

4:15pm **Dr. Michael Carter**
"Molecular Testing of Borderline Cutaneous Melanocytic Tumors: SNP Array is More Sensitive and Specific than FISH"

4:30-5:45 **DINNER AND POSTER SESSION**

5:45-6:30 **PLATFORM SESSION** (Moderators: Drs. Hema Ketha and Russell Ryan)

5:45pm **Dr. Stephanie Skala**
"FOXI1 is a Sensitive and Specific Marker for Detection of Primary and Metastatic Chromophobe Renal Cell Carcinoma"

6:00pm **Dr. Michael Bachman**
"Identification of Pathogenicity-Associated Loci in Klebsiella pneumoniae from Hospitalized Patients"

6:15pm **ABSTRACT AWARDS -** (Dr. Charles Parkos)

6:30-7:15pm **Introduction of Keynote Speaker - (**Dr. Aaron Udager)

KEYNOTE SPEAKER: Dr. Pedram Argani
Breast Pathology Director
Professor of Pathology and Oncology
Department of Pathology
Johns Hopkins Hospital

"MiT Family Translocation Carcinomas of the Kidney"

7:15-7:30pm **Q&A** (Moderator: Drs. Rohit Mehra and Scott Tomlins)

7:30pm **ADJOURN**

Platform Presentations

GIESEN AWARDEE LECTURE:

#1 - Metaplastic Breast Carcinomas Exhibit Low CCN6 Expression with Activation of the IGF2BP2-HMGA2-Signaling Axis

Emily R McMullen, Stephanie L Skala, Dafydd Thomas, Maria E Gonzalez, Celina G Kleer

Funded by: R01CA125577 from the NIH/NCI.
Manuscript: In preparation

Background: Metaplastic breast carcinomas are triple negative cancers with poor outcomes, displaying metaplastic components including spindle, squamous, and/or chondroid. Our lab has shown that CCN6 is a secreted protein that regulates the epithelial phenotype in the breast in part by reducing insulin-like growth factor (IGF) signaling. We recently generated mammary -specific MMTV-cre;Ccn6 knockout mice (CCN6 KO) that developed mammary tumors recapitulating human spindle metaplastic carcinomas. Through transcriptional profiling of mouse and human metaplastic carcinomas, the two most commonly upregulated genes were IGF2BP2 (insulin-like growth factor 2 mRNA binding protein 2) and its pathway protein HMGA2 (high mobility group AT-hook 2). These genes have been shown to promote migration in cancer, and are regulated by activation of the IGF type 1 receptor (IGF1R) and the insulin receptor (InsR). We hypothesize that CCN6 expression may be low in human metaplastic spindle cell carcinomas in association with upregulated IGF2BP2 and HMGA2 expression. We also hypothesize that secreted CCN6 may regulate the IGF2BP2-HMGA2 axis through inhibition of IGF signaling.
Design: We retrieved 31 metaplastic carcinomas resected from 1988-2015 at our institution. Tumors were reviewed and used to develop a tissue microarray (TMA), in duplicate. Immunohistochemistry (IHC) for CCN6, HMGA2, and IGF2BP2 were performed on TMA sections. IHC for HMGA2 and IGF2BP2 were performed on CCN6 KO mouse metaplastic carcinomas (n=6), and normal mouse mammary glands (n=10). Expression for CCN6 was evaluated as either low or high expression. Expression for IGF2BP2 and HMGA2 was assessed on a four-point scale (0, 1, 2, 3), and staining ≥1 was considered positive. High-grade human breast cancer cell lines with spindle morphology and low CCN6 expression, MDA-MB-231 and MDA-MB-436, were transduced with lentivirus-CCN6 or controls. Co-immunoprecipitation and Western blots were used to test binding between CCN6, IGF1R and InsR.
Results: All CCN6 KO mouse metaplastic carcinomas expressed high IGF2BP2 and HMGA2. No expression was detected in the normal mammary mouse epithelium. Low CCN6 was seen in the majority of human metaplastic carcinomas (27/31, 87%). All metaplastic carcinomas with a predominant spindled or squamous component showed low expression of CCN6. High CCN6 expression was seen in 4/31 cases (13%), all with chondroid predominant component. Ten of the 27 (37%) tumors with low CCN6 had concordant IGF2BP2 and HMGA2 expression, compared to 3/31 (10%) having low CCN6 and no IGF2BP2 and HMGA2 expression. Similar to mouse mammary glands, IGF2BP2 and HMGA2 were negative in the normal epithelium adjacent to tumor. We found that upon CCN6 overexpression in MDA-MB-231 and -436 cells, CCN6 co-immunoprecipitated with IGF1R and InsR at the cell membrane of cancer cells, resulted in a reduction of IGF2BP2 and HMGA2 levels compared to controls.
Conclusion: Low CCN6 and concordant upregulation of IGF2BP2 and HMGA2 identify a subset of human metaplastic carcinomas with spindled and/or squamous components. CCN6 regulates the expression of IGF2PB2 and HMGA2 in CCN6 KO mice and in breast cancer cell lines with spindled morphology. CCN6 binds to IGF1R and InsR, which may be a mechanism of CCN6-mediated regulation of the IGF2BP2-HMGA2 axis. CCN6 KO mice constitute a good model to study the pathogenesis of spindle metaplastic carcinomas with IGF2BP-HMGA2 axis activation, the tumor suppressor role of CCN6, and to test novel treatment strategies in this subset of aggressive tumors.

#2 - A Generalizable Deep Learning Model for Extraction of Diagnostic Data from Histopathological Data Sets

Ulysses J. Balis, Jerome Y. Cheng, David McClintock

Manuscript: In preparation

Background: Recent advances in morphological classification algorithms for histology have simplified the process of extracting reproducible archetypes of diagnostic features that tightly correlate with feature assignments, as generated manually by subject matter experts. One such family of algorithms, including Spatially Invariant Vector Quantization (SIVQ) and Validated Idempotent Pattern Recognition (VIPR), have demonstrated robust kappa statistic performance, as compared to conventional human-based feature classification.
Methods: When multiple orthogonal individual features vectors of the above algorithm family are utilized for the initial boundary conditions of machine learning classifier algorithms, and specifically, deep learning approaches, the resultant computational pipeline in many cases will allow for the expedited generation of a scalable image analysis algorithm that will perform, in addition to the initial training set, equally well upon a library of novel images, which themselves were not utilized in the initial training of the algorithm. Consistent generalizability of image-based computational algorithms has not been previously reported.
Results: With this effort, such generalizability for diagnostic feature extraction of renal biopsies is observed, demonstrating ROC data, which in nearly all cases exceeds 0.90. Similarly, the ability to computationally generate differential diagnoses is also made possible by these same computational pipelines, with preliminary efforts directed at chronic kidney disease and acute kidney injury demonstrating initial successes with the extraction of meaningful qualitative and quantitative diagnostic data.

#3 - Development of a Whole Urine, Next Generation Sequencing-Based Assay for Early Detection of Aggressive Prostate Cancer

Andi K. Cani, Sumin Han, Daniel H. Hovelson, Javed Siddiqui, Komal Kunder, Chia-Jen Liu, Simpa Salami, Todd M. Morgan, John T. Wei, Arul M. Chinnaiyan, Scott A. Tomlins

Manuscript: In preparation

Despite advances in biomarker development and imaging, early detection of aggressive prostate cancer (PCa) remains challenging. Existing non-invasive biomarkers show only modest improvement over models based on prostate specific antigen (PSA) and/or clinicopathological features. We have previously discovered, developed and/or validated multiple PCa- and aggressive PCa-transcriptomic tissue biomarkers, including coding genes, gene fusions and long non-coding RNAs (lncRNA). Likewise, we have developed a clinical laboratory developed test (LDT) for individualized risk prediction of aggressive prostate cancer risk termed MiProstate Score (MiPS), which quantifiesTMPRSS2:ERG (T2:ERG) and PCA3 from post-digital rectal exam (DRE) whole urine combined with serum PSA. To improve upon MiPS, here we describe the pre-clinical development of a targeted next generation sequencing (NGS)-based assay on RNA isolated from post-DRE urine to asses a set of ~90 PCa transcriptomic biomarkers, including those in MiPS as well as additional candidate biomarkers. Results from optimization of isolation and sequencing of over 200 post-DRE urine samples will be presented. Initial sequencing of 60 samples showed that 47 (78%) passed stringent QC filters. Replicate runs, including reruns of the same sequencing library, different libraries from the same RNA and different RNA extractions from the same urine sample showed excellent concordance (Pearson median r = 0.99). Importantly, urine NGS (uMiPS_v1) derived T2:ERG scores were highly concordant with MiPS T2:ERG scores (Pearson r = 0.83), while MiPS_v1 enabled quantification of additional T2:ERG fusion isoforms. Results from updated panels (uMiPS_v2 and _v3) and application to an extreme design cohort (benign/Gleason score 6 vs. Gleason score ≥ 4+3=7 samples) will be presented. Taken together, our results support the potential utility of a urine based targeted NGS assay to supplement PSA and clincopathological models for aggressive prostate cancer early detection.

#4 - Cytogenomic Array Detects a High-Risk Subset of Myelodysplastic Syndrome Invisible to Conventional Karyotype

Steven B Van Norman, Sarah M Choi, Lina Shao

Manuscript: In preparation

Background: Prognostic classification of myelodysplastic syndrome (MDS) using cytogenetic anomalies is currently utilized to guide therapeutic decision making—including the potential use of aggressive therapies such as bone marrow transplantation. Single nucleotide polymorphism arrays (SNP-As) have emerged as a potential means of further categorizing prognostic risk beyond traditional karyotyping in many hematologic malignancies due to the assay's greater sensitivity in detecting unbalanced chromosomal defects and copy-neutral loss of heterozygosity. However, widespread adoption and incorporation into prognostic algorithms remains limited.

Design: To assess the prognostic potential of SNP-As in MDS, we retrospectively reviewed 108 consecutive patients who underwent karyotyping and SNP-A analysis for diagnosis/classification of a suspected myeloid neoplasm (MDS or MDS/MPN). Overall survival was compared between patients with both low-risk karyotype (very good and good cytogenetic risk group) and consistent SNP-A, and patients with similar low-risk karyotype but abnormal SNP-A. These groups were compared to patients with abnormal karyotype stratified by the Revised International Prognostic Scoring System (IPSS-R) and to patients with abnormal karyotype stratified by known genetic risk factors (intermediate, poor, very poor cytogenetic risk groups). Mantel-Cox and Gehan-Breslow-Wilcoxon tests were used to compare overall survival between the groups.

Results: We found 45 patients with low-risk karyotype; SNP-A did not detect additional abnormalities beyond the karyotype in 23 patients and additional SNP-A abnormalities were detected in the remaining 22 patients. The additional SNP-A abnormalities were associated with significantly poor overall survival (p=0.0483). Patients with low-risk karyotype and additional abnormal SNP-A were found to group similarly to patients with poor – very poor risk karyotype and with high-very high IPSS-R, while patients with low-risk karyotype alone were found to group similarly to patients with very good-intermediate risk karyotype and with very low-intermediate IPSS-R (p=0.0117).

Conclusion: SNP-As, when used with traditional karyotyping methodology, can more accurately predict overall survival than karyotyping alone. This is especially cogent to patients with a normal karyotype who may harbor poor risk genetic alterations undetectable by traditional karyotyping. These patients would potentially benefit from therapeutic plans informed by more accurate prognosis.

#5 - Molecular Testing of Borderline Cutaneous Melanocytic Tumors: SNP Array is More Sensitive and Specific than FISH

Michael D. Carter, Paul W. Harms, May P. Chan, Rajiv Patel, Lori Lowe, Douglas R. Fullen, Alex Hristov, Min Wang, Aleodor A. Andea

Presented at: Accepted as platform presentation at upcoming USCAP 2018 Annual Meeting
Manuscript: In preparation

Background: Melanocytic lesions with borderline features are diagnostically challenging. Molecular techniques based on detection of genomic copy number alterations (CNA) using single nucleotide polymorphism (SNP) arrays can be helpful in predicting whether a lesion is likely to behave in an indolent or aggressive manner (i.e. like a nevus or a melanoma). Fluorescence in situ hybridization (FISH) has been used as a more rapid, less expensive alternative to SNP array, employing a panel of probes that may be gained (*RREB1*, *MYC*, *CCND1*), or lost (*MYB,* homozygous *CDKN2A* loss) in melanoma. While the sensitivity and specificity of FISH testing are both reported to be in excess of 90%, validation studies are based on well-characterized nevi and melanoma rather than borderline melanocytic tumors.
Design: We used SNP array data from 63 borderline cutaneous melanocytic lesions and 45 definitive melanomas, which served as a control group, to predict the performance of FISH testing. Lesions were considered positive by "virtual FISH" if one or more of the 5 FISH-probed loci demonstrated appropriate CNAs by SNP array. Cases were classified as positive by SNP array if 3 or more CNA (>3 MB each) were present, or if the FISH criteria were met. Additionally, lesions which had only gains or losses of entire chromosomes were designated as negative, regardless of changes at the FISH loci, as this pattern is characteristic of benign proliferative nodules. Conventional FISH was performed in 31 cases.
Results: Of the 63 borderline cases, 44 (70%) were positive by SNP array and 29 (46%) were positive by virtual FISH. A higher proportion of melanomas were positive by SNP array (42/45, 93%) and virtual FISH (36/45, 80%). Compared to SNP array, virtual FISH failed to recognize 19 cases with concerning CNAs (false negatives, Fig. 1A) and incorrectly classified as positive 3 cases with whole chromosome gains and losses (false positives, Fig. 1B). Sensitivity of virtual FISH compared to SNP array was 86% in the melanoma group but only 57% in the borderline group, while specificity was 100% and 84% in these groups, respectively. There was good correlation between conventional and virtual FISH, with agreement in 18/19 conventional FISH positive and 11/12 negative cases.

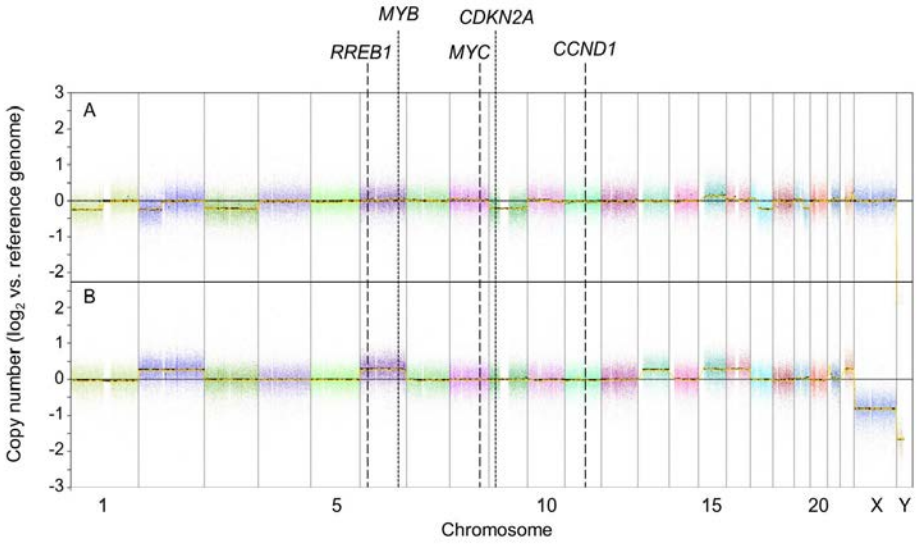

Fig. 1. SNP arrays showing examples of borderline melanocytic lesions with false negative and false positive virtual FISH results. A, False negative case in which 8 copy number aberrations are present, consistent with an aggressive lesion, but negative by FISH (only heterozygous loss of *CDKN2A*). B, False positive case in which only whole chromosome gains (2, 6, 13, 15,16, 22) and loss (X) are present, consistent with a benign proliferative nodule, despite a positive result by FISH (copy number gain of *RREB1*). FISH loci indicated by dashed lines (gains associated with melanoma) and dotted lines (losses associated with melanoma, with only homozygous *CDKN2A* loss considered positive).

Conclusions: While FISH is highly effective in distinguishing between nevi and melanoma in cases where the histological diagnosis is straightforward, it is not nearly as sensitive or specific as SNP array when applied to borderline melanocytic lesions.

#6 - FOXI1 is a Sensitive and Specific Marker for Detection of Primary and Metastatic Chromophobe Renal Cell Carcinoma

Stephanie L Skala, Lisha Wang, Yuping Zhang, Sathiya P Narayanan, Xuhong Cao, Javed Siddiqui, Cieślik Marcin, Arul M Chinnaiyan, Saravana M Dhanasekaran, Rohit Mehra

Presented at: MSP
Manuscript: In preparation

Background: The immunohistochemical (IHC) stains commonly used to support the diagnosis of chromophobe renal cell carcinoma (RCC) are not lineage-specific and are expressed by multiple tumors arising from various organs. Discovery of cancer-specific markers will alleviate challenges related to evaluation of metastases or tumors with unusual morphology.
Design: We analyzed RNA sequencing data from a cohort of 1049 RCC specimens from The Cancer Genome Atlas, several in-house rare RCC specimens, and microdissected mouse nephron to identify cancer/lineage-specific biomarkers. We built a webportal ("Renaissance") for data visualization and nominated lineage-specific biomarkers including FOXI1. For validation, we performed IHC with an anti-FOXI1 antibody to assess the FOXI1 expression status of tumors retrieved from the surgical pathology database at our large academic institution including classic chromophobe RCC (n= 33), eosinophilic chromophobe RCC (n=10), unclassified RCC with oncocytic features (n= 6), clear cell RCC (6 grade 2, 10 grade 3, 14 grade 4), clear cell papillary RCC (n=5), mucinous tubular and spindle cell carcinoma (MTSCC, n=1), and papillary RCC (6 type 1, 4 type 2). All available chromophobe RCC metastases were retrieved (n=17), as well as clear cell RCC (n=16) and papillary RCC metastases (n=5) from various sites.
Results: All primary and metastatic chromophobe RCC demonstrated diffuse nuclear FOXI1 expression. Eosinophilic chromophobe RCC and unclassified RCC with oncocytic features also demonstrated positive nuclear FOXI1 expression. In contrast, no clear cell RCC (primary or metastatic), clear cell papillary RCC, papillary RCC (primary or metastatic), or MTSCC showed nuclear FOXI1 expression.
Conclusion: Based on our findings, nuclear FOXI1 expression is highly sensitive and specific for variants of chromophobe RCC and other RCC with oncocytic features in primary and metastatic settings. Our results suggest that the cell of origin for chromophobe RCC resides in the connecting tubule/collecting duct of the nephron.
.

#7 - Identification of Pathogenicity-Associated Loci in *Klebsiella pneumoniae* from Hospitalized Patients

Rebekah M. Martin, Jie Cao, Weisheng Wu, Lili Zhao, David M. Manthei, Ali Pirani, Evan Snitkin, Preeti N. Malani, Krishna Rao, Michael A. Bachman

Despite insights gained through experimental models, the set of bacterial genes important for human infection is unclear for many of our most threatening pathogens. *Klebsiella pneumoniae* is a leading cause of healthcare-associated infections (HAI) and commonly colonizes hospitalized patients, but the factors that determine whether a particular isolate causes disease or remains a colonizer are poorly understood. To identify bacterial genes associated with *K. pneumoniae* infection, a case-control study was performed comparing infected and asymptomatic colonized patients. Comparative bacterial genomics was combined with a conditional logit model that identified patient factors differentiating cases from controls. This method identified five gene loci associated with infection after adjustment for patient factors, including a psicose sugar utilization that was a fitness factor during mouse lung infection. These results indicate that bacterial genome-wide association studies of patients can identify loci associated with HAIs and important in infection models.

Poster Presentations

#1 - Pediatric Thyroid Fine Needle Aspiration: Experience of a Tertiary Care Referral Center

Stacy J Arnold, Amer Heider, Xin Jing

Presented at: Will be presented at USCAP2018
Manuscript: In preparation

Background: Thyroid nodules in children carry a higher risk of malignancy than those in adults. Fine needle aspiration (FNA) has been essential in the evaluation and workup of thyroid nodules; however, there are few publications in the medical literature discussing thyroid FNA in the pediatric population. The American Thyroid Association (ATA) has put forth guidelines for best practice management of pediatric thyroid nodules with the goal of minimizing morbidity and mortality in this age group.

The main goal of this study is to evaluate our experience with pediatric thyroid FNA using the Bethesda System for Reporting Thyroid Cytology (BSRTC) including cytologic-histologic correlation at our large referral center. A secondary aim is to compare our malignant surgical outcome results based on FNA diagnostic categories with the 2015 ATA guidelines.

Design: A retrospective data search was conducted between 1/1/2011 and 8/31/2017 to identify thyroid FNA samples obtained from patients under 21 years of age. FNA results were recorded using the BSRTC diagnostic categories. Follow-up surgical intervention data was obtained where available. Statistical analysis of the data including the risk of malignancy per diagnostic category and rates of cytologic-histologic correlation were calculated.

Results: 169 FNA specimens were retrieved from 126 patients. More than half of the patients underwent surgical intervention (Table 1).

One patient with a non-diagnostic FNA had malignancy on excision. All of the positive aspirates having surgical follow-up showed malignant histology (Table 2). Concordance rate was excellent for the negative, suspicious, and positive categories. Follicular lesion of undetermined significance cases had a 23.1% malignancy rate.

Results:

Table 1. Demographics	
Number of patients	126
Number of FNAs	169
Female to Male ratio	5.3:1
Age range	5-20 yrs
Thyroidectomy	67
Hemi-thyroidectomy	27
Total thyroidectomy	40

Conclusion: The data from our large institution supports the utility of thyroid FNA and the efficacy of the BSRTC in children and adolescents, and is in alignment with previously published data. The high concordance rate, sensitivity and specificity emphasize how effective BSRTC categorization is for risk stratification of pediatric thyroid nodules. Further, our data is in keeping with the ATA task force findings, specifically regarding the higher risk of malignancy (15-30%) on surgical excision of indeterminate nodules (FLUS/AUS) in the pediatric population as compared to adults (5-15%).

Table 2 Diagnostic category	N(%)	Surgical f/u (%)	Concordance N (%)	Malignant Outcome N (%)
1 - Non-diagnostic	12/169 (7.1)	9/12 (75)	-	1/9 (11.1)
2 - Benign	98/169 (58)	31/98 (31.6)	27/31 (87.1)	0/31 (0)
3 - FLUS/AUS	15/169 (8.9)	13/15 (86.7)	5/13 (38.5)*	3/13 (23.1)
4 - SFN/FN	8/169 (4.7)	7/8 (87.5)	7/7 (100)*	1/7 (14.3)
5 - SFM	7/169 (4.1)	7/7 (100)	7/7 (100)*	6/7 (87.5)
6 - Malignant	29/169 (17.2)	28/29 (96.6)	28/28 (100)^	28/28 (100)

*Histology confirmed neoplasm/malignancy
^Histology confirmed malignancy
FLUS- Follicular lesion of undetermined significance,
AUS - Atypia of undetermined significance,
SFN - Suspicious for follicular neoplasm,
FN -follicular neoplasm,
SFM - Suspicious for malignancy

#2 - A Digital Image Analysis Tool for Automated Scoring of IHC Stains and Classification of Diffuse Large B-cell Lymphoma Sub-types Based on Hans Algorithm

Muhammad N Aslam, Srikanth Ragothaman, Rajan Dewar

Presented at: CAP2018
Manuscript: In preparation

Background: Activated B-cell (ABC) and Germinal Center B-cell (GCB) are the two cell of origin (COO) based sub-types of Diffuse Large B-cell Lymphoma (DLBCL), and are shown to have prognostic value. Subsequent to the original Gene Expression profiling study, a simple immunostain based algorithm (Hans) has been widely used to aid in the sub-typing of DLBCL. The Hans algorithm is based on three immunostains: CD10, BCL6 and MUM1. Despite the simplicity, Hans algorithm suffers from several pitfalls: variability of immunostains, inter-observer variations in stain interpretations and failure to correlate with outcome, in as much as 22% of DLBCL cases. We have developed an automated image analysis based algorithm (EnHANS) which could be useful in classifying DLBCL.
Design: 11 cases of DLBCL from a well-curated cohort were included. H&E stains and immunostains for CD10, BCL6, and MUM1 were performed and scanned. The EnHANS platform was trained on static digital IHC images to recognize positive cells (CD10 – membrane staining; BCL6 and MUM1 – nuclear). Using a 30% threshold, the algorithm automatically subtyped the DLBCLs according to cell-of-origin. Two pathologists scored the whole slide and one pathologist scored digital images used by EnHANS to derive subtypes for all 11 cases, blinded to the EnHANS data. (Note: ABC term is used instead of Non-GCB for simplicity).
Results: The results are shown in Table/Figure 1 (discordances are highlighted). The concordance between EnHANS and pathologists is 82% (9/11 cases) for the DLBCL subtype, 82% (9/11) for CD10 expression, 64% (7/11) for BCL6 expression, and 100% for MUM1 expression. The majority of the discordances occurred where the percentages of positive cells as determined by EnHANS were close to the 30% threshold. In one case (#4), EnHANS failed to recognize staining artifact and misclassified the CD10 stain as positive. In another case (#11), a BCL6 stain was scored as "weak positive" and "negative" by the two pathologists and "positive" by EnHANS.
Results Table:

S.No.	CD10	BCL6	MUM1	EnHANS subtype
1	9.83	47.65	50.91	ABC
2	0.12	42.4	58.79	ABC
3	7.2	**46.14**	47.4	ABC
4	**30.66**	**43.94**	72.96	**GCB**
5	20.23	**43.65**	73.59	ABC
6	0.2	23.61	55.95	ABC
7	0.08	51.1	69.88	ABC
8	55.27	43.06	69.23	GCB
9	**28.02**	58.41	48.36	**ABC**
10	42.84	58.485	30.34	GCB
11	21.4	**41.04**	63.9	ABC

Conclusion: Image analysis tools may have a role in the automated classification of DLBCL subtypes, particularly in cases where the percentages of positive cells by IHC are close to established thresholds. We plan to refine the EnHANS algorithm by using additional cases from our curated cohort with correlation to human pathologist scores.

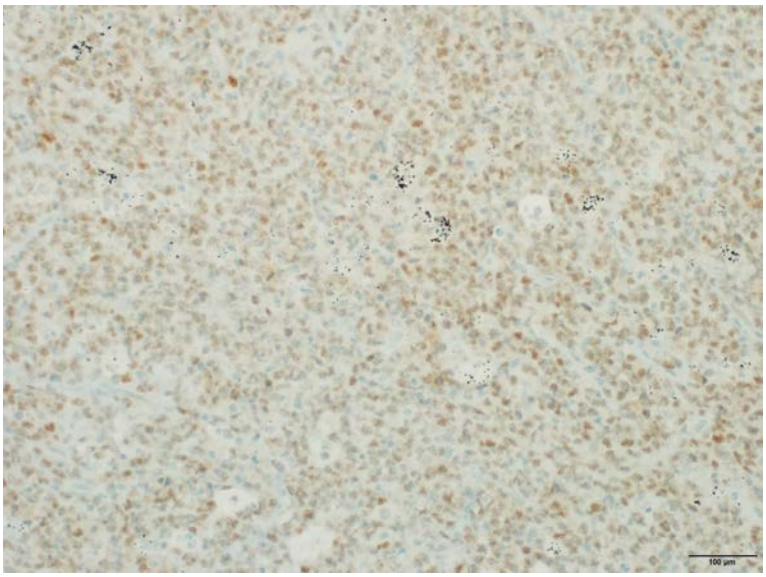

S.No.	CD10	BCL6	MUM1	Manual subtype	enHANS subtype
1	NEG	POS	POS	**ABC**	ABC
2	NEG	POS	POS	**ABC**	ABC
3	NEG	NEG	POS	**ABC**	ABC
4	ENG	NEG	POS	**ABC**	GCB
5	NEG	NEG	POS	**ABC**	ABC
6	NEG	NEG	POS	**ABC**	ABC
7	NEG	POS	POS	**ABC**	ABC
8	POS	POS	POS	**GCB**	GCB
9	POS	POS	POS	**GCB**	ABC
10	POS	POS	POS	**GCB**	GCB
11	NEG	NEG	POS	**ABC**	ABC

#3 - Aberrant CSF-1R Signaling is Associated with T-cell Lymphoma Progression: Implications for Therapeutic Targeting of Lymphoma-Microenvironment.

Noah Brown, Carlos Murga-Zamalloa, Avery Polk, Delphine Rolland, Ryan Wilcox

Background: Peripheral T-cell lymphoma (PTCL) is a poorly understood group of diseases. While significant therapeutic advancements have been achieved for the more common B-cell non-Hodgkin lymphomas, PTCL's are associated with inferior responses to therapy, dismal overall survival, and remain an unmet need. Lymphoma-associated macrophages are abundant constituents of the tumor microenvironment, and are critical components during T-cell lymphoma progression and chemotherapy resistance. We have recently show that a significant proportion of PTCL's (Anaplastic large cell lymphoma 'ALCL', Peripheral T-cell lymphoma non-otherwise specified 'PTCL-NOS', and Angioimmunoblastic T-cell lymphoma 'AITL') feature aberrant surface expression of the colony-stimulating factor 1 receptor (CSF-1R). Importantly, paracrine secretion of colony-stimulating factor-1 (CSF-1) by lymphoma-associated macrophages specifically occurs in the microenvironment of several types of lymphomas. Therefore, we decided to evaluate the oncogenic role of CSF-1R signaling in T-cell lymphomas. By means of pharmacologic and knock-down approaches, we have demonstrated that inactivation of CSF-1R in T-cell lymphoma lines prevents its growth during in-vitro and in-vivo experimental conditions. However, the specific mechanism of CSF-1R-dependent oncogenesis in T-cell lymphomas remains to be elucidated.

Results: In order to evaluate the aberrant activation of CSF-1R in T-cell lymphomas, we tested if autocrine secretion of CSF-1 was present among different T-cell lymphoma lines. Our findings show that several T-cell lymphoma lines feature secretion of CSF-1 ligand by ELISA immunoassay, suggesting that an autocrine loop is coupled with paracrine signals from lymphoma-associated macrophages during activation of CSF-1R-signaling. In order to fully understand the role of CSF-1R-dependent oncogenesis in T-cell lymphomas, we evaluated the gene-expression profile of T-cell lymphoma lines upon selective pharmacologic inhibition of CSF-1R with the novel tyrosine kinase inhibitory compound PLX3397. We have identified a large set of genes that are differentially regulated upon inhibition of CSF-1R, a subset of these genes are involved in lymphoma metabolism, growth and resistance to apoptosis. Our findings indicate that a unique subset of genes are specifically regulated downstream of CSF-1R signaling, as those do not feature changes in expression during inhibition of different signaling pathways involved in lymphoma progression, including ALK-signaling. To further evaluate the signals that are orchestrated downstream of CSF-1R, we performed an un-biased phosphoproteomic screening of ALK-positive ALCL cell lines upon selective inhibition of CSF-1R with PLX3397. We have identified that CSF-1R regulates the phosphorylation of proteins that are involved in tumor metabolism and growth, including AKT and GSK3β. We have further validated these results by western blot analysis in T-cell lymphoma lines with aberrant expression of CSF-1R.

Our previous findings show that selective CSF1R inhibition with PLX3397 administration to tumor-bearing mice, significantly impairs the growth of tumor xenografts in a "static" fashion. Therefore, given its restricted tissue expression in humans, CSF-1R may be an optimal therapeutic target in the T-cell lymphomas, particularly if its inhibition were "synthetic lethal" with an additional and targetable receptor or pathway. In order to identify clinically available therapeutic agents (e.g. tyrosine kinase or signaling pathway), that are synthetic lethal with PLX3397 in CSF-1R expressing malignant T cells we performed a chemical high-throughput screen using annotated drug libraries available at the Center for Chemical Genomics (CCG) at the University of Michigan. Our screening demonstrates that PLX3397 show synthetic lethality with different histone deacetylase inhibitory agents. To validate these results in-vitro, T-cell lymphoma lines were treated with the HDAC inhibitory agent romidepsin, in combination with CSF1R inhibition (PLX3397) or control (DMSO). Selective CSF1R inhibition coupled with romidepsin treatment showed decreased survival (IC50 = 0.60) when compared to romidepsin coupled with controls (IC50 = 0.88).

Conclusions: Our studies show that activation of the CSF-1 receptor (CSF-1R) regulates specific gene expression and proteomic phosphorylation events, orchestrating the activation of signals that promote T-cell lymphoma progression. These signaling events occur downstream of coupled autocrine and paracrine signals from lymphoma-associated macrophages, supporting a tight role of the tumor microenvironment during lymphoma progression. Our findings support future clinical interventions that will incorporate combination therapy with specific CSF-1R and HDAC inhibitors.

#4 - Clinical Utility of Large Scale Genomic Sequencing of Solid Tumors at a Large Academic Medical Center

Noah A. Brown, Gregory P. Kalemkerian, Mark M. Zalupski, Angel Qin, Nguyen Tran, Bryan L. Betz

Presented at: Association for Molecular Pathology (AMP)
Manuscript: In preparation

Introduction: FoundationOne is a commonly used molecular panel for screening solid tumors for both standard of care and investigational biomarkers. However, the clinical utility of this type of large-scale genomic profiling in place of standard of care molecular testing or testing using smaller, commericially-available NGS panels is uncertain.
Methods: FoundationOne reports were reviewed for all University of Michigan patients for whom FoundationOne testing was performed over a three-year period. All available medical oncology notes were reviewed for each patient to determine what action, if any, was taken on the basis of the results. Performance metrics including turn-around-time (TAT) and incidence of rejected (QNS; quantity not sufficient) or failed specimens were also recorded and compared with those obtained from University of Michigan experience with the Oncomine Focus Assay (Thermo Fisher Scientific).
Results: Testing was successful in 355 patients. The most common cancer types included colorectal cancer (CRC; 33.8%), non-small cell lung cancer (NSCLC; 17.5%), breast cancer (6.5%), ovarian cancer (5.9%), pancreatobiliary cancer (3.9%) and head and neck cancer (3.9%). Potentially actionable variants (based on FoundationOne reporting) were identified in 87.9% of samples and were classified as relevant for an FDA-approved therapy in the patient's tumor type (33.8%; 18.6% if *RAS* mutations in CRC are excluded), relevant for an FDA-approved therapy in another tumor type (60%), and relevant for clinical trials (87.0%). 42.5% of the first category were *RAS* mutation in CRC patients. FoundationOne results altered patient management in 47.3% of cases. However, 72.6% of these clinical actions reflect standard of care molecular findings (predominantly *RAS* mutation status in CRC patients). Excluding standard of care molecular findings, FoundationOne results altered patient management in 13.5% of patients. Of these, 43.8% (7.6% of total) were treated with an FDA-approved drug for an off-label indication, and 56.3% (5.9% of total) were enrolled in a clinical trial. All of the variants that affected patient management are included in the TruSight Tumor 170 Assay (Illumina), 99.2% are included in the Oncomine Comprehensive Assay v3 (Thermo Fisher Scientific) and 97.1% are included in the Oncomine Focus Assay (Thermo Fisher Scientific). FoundationOne testing had an average TAT of 11.4 days (range: 4 – 25 days) compared to 8 days (range: 5 – 14) for Oncomine Focus. The percentage of QNS/failed specimens was 12.6% for FoundationOne compared to 0.2% for Oncomine Focus.
Conclusions: The number of patients whose management is affected by FoundationOne sequencing results is far lower than the number variants designated actionable within FoundationOne reports and most variants affecting patient management reflect standard of care molecular analytes. In addition, most, if not all, variants that affect patient management are detectable using smaller, commercially available oncology panels that can be implemented in local clinical laboratories. These smaller panels may also have performance advantages that are important to patient care including shorter TAT and fewer QNS/failed specimens.

#5 - Targeted Genomic Profiling of *BRAF/KIT/NRAS* Mutation-Negative Gynecologic Melanoma Reveals Recurrent *NF1* Alterations and *TP53* Mutations

Cody S. Carter, Komal R. Kunder, Aleodor A. Andea, May P. Chan, Douglas R. Fullen, Lori Lowe, Scott A. Tomlins, Aaron M. Udager, Rajiv M. Patel

Presented at: Accepted for poster presentation at USCAP 2018
Manuscript: In preparation
Funding: AP Project Funding Committee

Background: Gynecologic melanomas (GM), including those involving the vulva, vagina, and/or cervix, are uncommon, aggressive tumors with poor long-term clinical outcome. Our group recently reported a relatively low rate of mutations (<30%) in conventional melanoma oncogenes (*BRAF*, *KIT*, and *NRAS*) in a large retrospective cohort of GM. In this study, we utilized targeted next-generation DNA sequencing (DNAseq) to characterize the genomic landscape of *BRAF*/*KIT*/*NRAS* mutation-negative ("triple-negative") GM.
Design: Four "triple-negative" GM at a single large academic institution were retrospectively identified from a previously published tumor cohort. Representative formalin-fixed paraffin-embedded tissue was selected for targeted DNAseq using the Oncomine Comprehensive Assay and an Ion Torrent Proton sequencer. Somatic variants and copy number alterations (CNA) were identified via in-house bioinformatics pipelines, and prioritized alterations were nominated by manual curation using previously established criteria.
Results: Overall, a total of 7 prioritized somatic variants were identified (median per tumor = 2; range = 0-3), including *TP53* (*n* = 3), *NF1* (*n* = 1), and *NOTCH1* (*n* = 1) mutations; no *SF3B1* mutations were identified. A total of 20 CNA were identified (median per tumor = 3; range = 2-12), including recurrent *NF1* (*n* = 3) and *CDKN2A* (*n* = 2) deletions. One tumor showed focal 4q12 amplification (including *PDGFRA*, *KIT*, and *KDR*) with concurrent amplification of *MTOR*, while one tumor each demonstrated focal *CDK4* and *MYCL* amplification. Integrating somatic variant and CNA data, all tumors showed one or more *NF1* alteration, and half of tumors demonstrated *TP53* mutation with concurrent *CDKN2A* deletion.
Conclusion: "Triple-negative" GM show recurrent *NF1* alterations, including frequent deletion and occasional somatic mutation, indicating that altered NF1 activity likely plays a central pathogenic role in these tumors. Concurrent tumor suppressor alterations, including *TP53* mutations and/or *CDKN2A* deletions, and focal non-recurrent amplifications are also frequently observed. Overall, these data suggest that, despite the absence of conventional oncogenic mutations (*BRAF*, *KIT*, and *NRAS*), downstream activation of the RAS/RAF and/or PI3K/AKT pathways is common in "triple-negative" GM and may be therapeutically targetable.

#6 - Genome-Wide Copy Number Aberration and Targeted Next-Generation Sequencing Studies of Merkel Cell Carcinoma

Michael D. Carter, Daniel Gaston, Weei-Yuarn Huang, Wenda Greer, Sylvia Pasternak, Thai Yen Ly, Noreen M. Walsh

Presented at: Association for Molecular Pathology 2017 Annual Meeting, Nov. 24 2017
Manuscript: In press
Funding: Nova Scotia Health Authority Research Fund

Tumorigenesis in Merkel cell carcinoma (MCC) is driven by (i) clonal integration of the Merkel cell polyomavirus (MCPyV) in neoplastic cells and/or (ii) genetic damage by ultraviolet (UV) light. A higher mutational burden, a UV-mutational signature, and many mutations in the *TP53* and *RB1* genes characterize the virus-negative subset. MCPyV-negative MCCs include combined (often squamous and neuroendocrine) and pure (neuroendocrine) tumors. Because a combined morphology could elude detection microscopically, we sought a genetic link between combined and pure virus-negative tumors. From a global cohort of 46 cases, 9 pure MCPyV-positive, 9 pure MCPyV-negative, and 10 combined MCPyV-negative MCCs were studied by genome-wide microarray in search of copy number aberrations (CNAs). The entire cohort (n=46) was evaluated by next-generation sequencing (NGS) for mutations in selected tumor suppressor genes and oncogenes. More CNAs and a greater fraction of the genome was changed in combined and pure MCPyV-negative tumors relative to MCPyV-positive cases (P<.01 for all comparisons). No difference in these parameters was found between the two MCPyV-negative groups. Copy number loss of *RB1* or an inactivating *RB1* mutation (either or both) was common in combined (8/10, 80%) and pure (7/9, 78%) MCPyV-negative tumors, but not MCPyV-positive cases (1/9, 11%). A similar trend was seen for *TP53*, [combined (2/10, 20%) and pure virus-negative tumors (5/9, 56%) showed gene copy number loss or mutations, contrasted with pure virus positive cases (0/9, 0%)]. The shared genetic profiles of combined and pure MCPyV-negative tumors link these subsets and separate them from MCPyV-positive tumors.

#7 - Rapid Progression of Myelodysplastic Syndrome to Acute Myeloid Leukemia is Associated with Acquired Somatic Mutations in *KRAS*

Nathan J Charles, Shannon D McClintock, James Varani

Presented at: Beaumont Hospital's 26th Annual Symposium for Molecular Pathology: Clinical Applications of Genomic Medicine (Sept. 2017)
Manuscript: In preparation, pending follow up studies

Myelodysplastic syndrome (MDS) is a clonal and genetically heterogeneous primary bone marrow disorder characterized by ineffective hematopoiesis and progression to acute myeloid leukemia (AML) in up to one third of patients. Recent studies have shown temporally acquired genetic mutations in MDS increases the risk for leukemic transformation. Therefore, our goal was to identify and characterize dynamically acquired driver mutations from paired MDS and AML bone marrow samples that may be responsible for more rapid disease progression and worse patient outcome.

Using an unbiased cancer hot spot next generation sequencing panel, paired bone marrow samples from AML patients with antecedent MDS were analyzed and compared for genetic mutation acquisition. High resolution melting curve analysis and pyrosequencing were used as rapid methods of mutation confirmation. Phospho-kinase array screening was implemented to identify potential downstream effectors for further investigation in transgenic MDS cell lines.

Activating point mutations in *KRAS* were temporally acquired in 4 of 11 patients who also progressed to AML at significantly faster rates than those who remained *KRAS* wild-type ($p \leq 0.05$) (Fig. 1). *KRAS* mutational burden within bone marrow and peripheral blood samples was directly proportional to disease progression as measured by high resolution melting curve analysis (Fig. 2). Analyzing the activation status of 43 distinct kinases showed increased CREB phosphorylation, a downstream effector of KRAS signaling. Furthermore, immunohistochemistry revealed significantly increased expression of the CREB transcriptional target and pro-survival factor BCL-2 ($p \leq 0.05$). Subsequently established transgenic MDS cell lines possessing inducible mutant *KRAS* (G12V) preliminarily demonstrate increased survival as compared to wild-type control.

Using next generation sequencing and high resolution melting curve analysis, we have established a paradigm for identifying dynamically acquired and patient specific driver mutations followed by rapid monitoring of mutational burden. Specifically, acquired gain of function *KRAS* mutations are associated with significantly faster AML progression rates potentially mediated via CREB activated transcriptional control of *BCL-2*. Therefore, early detection and targeted disruption of the KRAS-CREB-BCL-2 pathway may lengthen or altogether prevent leukemic transformation in MDS patients who acquire *KRAS* mutations during the course of their disease.

#8 - Frozen Section Experience for Breast Conserving Therapy: Analysis of Frozen Section Discrepancies

Ellen East, Cody Carter, Arielle Kanters, Celina Kleer

Background: Intraoperative frozen section of breast tissue for margin analysis (FSM) decreases reoperation in women undergoing breast conserving therapy. False negative margins due to sampling error (SE) or interpretive error (IE) may occur in lesions with subtle gross or histologic findings, such as carcinoma in situ or invasive lobular carcinoma. We aim to characterize cases where frozen section analysis fails to correctly characterize margins with the goal of reducing reoperation.
Methods: Key word search identified cases over a 1 year period, 2016-2017. Clinicopathologic features including age, diagnosis, number of parts and blocks submitted for FSM, margin status, discrepancy between margin status at frozen and final report, surgery location, turn around time, and re-excision were recorded.
Results: 296 specimens from 276 patients were identified, including 37 re-excision specimens. Mean age was 58.6 (range 17-85) and 275 (99.6%) were female. Specimens included lumpectomies (246, 83.1%), excisions (43, 14.5%) and mastectomies (7, 2.4%). A median of 1 part (range 1-8) and 4 blocks (range 1-24) were submitted for FSM. Most surgeries (228, 77.0%) were performed at an ambulatory surgical center (ASC) that only performs breast FSM, while a subset (68, 23.0%) were done at a large hospital that performs frozen section for all surgical specialties. Of malignant cases (n=245), 184 (75.1%) had negative margins and 62 had close and/or positive margins for in situ and/or invasive disease. 47 (15.9%) cases had FSM discrepancy, which was attributed to SE (41, 87.2%), IE (4, 8.5%) or both SE and IE (2, 4.3%). SEs were found on additional blocks for permanents (20, 42.6%), deeper sections of frozens (14, 29.8%), or both deeper and additional sections (3, 6.4%).High grade DCIS was the most common diagnosis in FSM discrepant cases, followed by IDC grade 2-3 and ILC (any grade) (Table 1). FSM discrepancy was not related to number of parts (p=0.532) or blocks submitted (p=0.420). TAT at the ASC was lower (35 min, range 11-120) than at the main hospital (42 min, range 13-138, p=0.011). There was no difference in parts (p=0.53) or blocks (p=0.42) submitted between sites.
Discussion: While in most cases frozen section accurately assesses margin status, SE is the main cause of discrepancy for in situ and invasive disease. Cases of high grade DCIS, grade 2-3 IDC, and ILC are overrepresented in FSM discrepancies. These results will help optimize frozen section sampling to accurately assess margins in such cases.

Table 1. FSM discrepant cases with positive margins, n=47

	Close	Positive
Carcinoma in situ		
High grade DCIS	14	4
Intermediate grade DCIS	7	1
Low grade DCIS	2	0
DCIS grade not specified	1	0
Pleomorphic LCIS	1	0
Invasive carcinoma		
Invasive ductal carcinoma	9	2
Grade 1	1	1
Grade 2	4	0
Grade 3	3	1
Grade not specified	1	0
Invasive ductal carcinoma with lobular features	1	0
Grade 1	1	0
Invasive lobular carcinoma	4	2
Grade 1	1	0
Grade 2	2	0
Grade not specified	1 (residual)	2 (residual)

#9 - Expression and Prognostic Value of NSD1 and SETD2 in Pancreatic Ductal Adenocarcinoma (PDA) and its Precursor Lesions

Mark Ettel, Shula Schechter, Lili Zhao, Jiaqi Shi

Presented at: Accepted for USCAP 2018
Funded by: AP Project Funding Committee
Manuscript: In preparation

Background: Epigenetic regulation has been emerging as a critical mechanism for PDA development. Many epigenetic regulator genes are altered and considered as drivers in PDA. Histone methylation is one of the most important mechanisms of epigenetic regulations. These modifications can alter chromatin structure and promoter accessibility, and thus lead to aberrant gene expression. Recent genomic sequencing studies showed that NSD1 and SETD2, genes encoding two histone H3K36 methyltransferases, are mutated or altered in about 10% of PDA cases. However, whether there is altered protein expression of NSD1 or SETD2 in PDA and its precursors, and whether they have diagnostic or prognostic utility is not known.
Design: Tissue microarrays (TMAs) composed of a total of 190-195 duplicated cases of PDA (n=74-75), metastatic PDA (n= 17-18), pancreatic intraepithelial neoplasia (PanIN; n=19-25), intraductal papillary mucinous neoplasm (IPMN; n=36), mucinous cystic neoplasm (MCN; n=12) and benign pancreatic tissues (n=29-32) were analyzed for expression of NSD1 and SETD2 by immunohistochemistry. We assessed intensity (0, 1, 2, 3), and percentage of positive cells (score=intensity x % positive cells). Overall and progression-free survival was compared between NSD1/SETD2-low and high expression patients using Kaplan-Meier analysis.
Results: Both NSD1 and SETD2 showed a trend toward either increased (NSD1) or decreased (SETD2) protein staining in PDA/metastatic PDA and its precursor lesions compared to benign ducts. In addition, decreased expression of SETD2 appears to be a slightly favorable independent prognostic factor for progression-free survival of PDA. However, these findings did not reach statistical significance (p=0.1 and p=0.4955), probably due to the variability of the protein levels in dysplastic/neoplastic lesions. [Table 1][Figure 1]
Conclusion: Expression of NSD1 and SETD2 are altered in some cases of PDA and its precursor lesions, supporting their important role in PDA development. Decreased expression of SETD2 is associated with a slightly favorable outcome in PDA. However, these findings did not reach statistical significance.

Figure 1. Kaplan-Meier progression-free survival curve

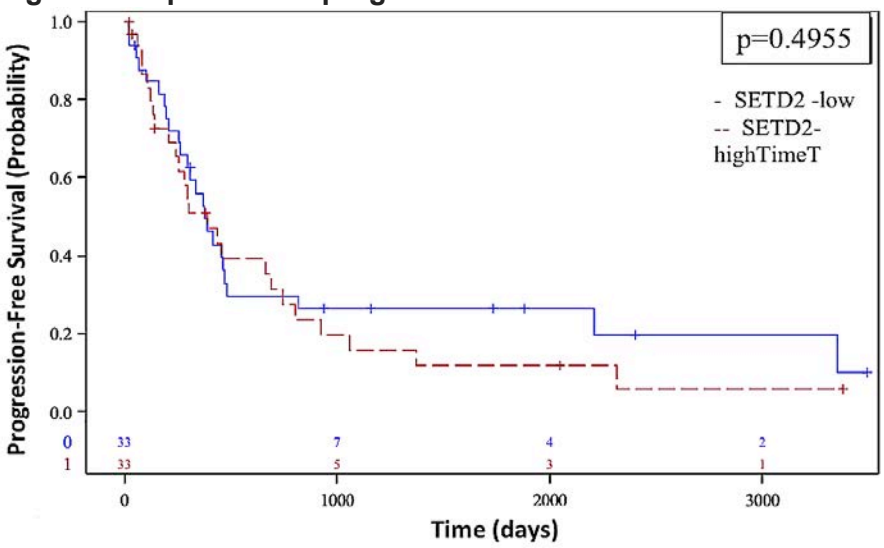

Table 1. Expression of NSD1 and SETD2 in PDA and its precursors

Diagnosis	NSD1 score (Mean ± SD)	SETD2 score (Mean ± SD)
Normal	78.3 ± 47.5	176.6 ± 58.8
PanIN	83.2 ± 65.2	134.2 ± 47.4
IPMN	99.4 ± 57.8	167.5 ± 61.1
MCN	83.3 ± 73.9	125.8 ± 65.3
PDA (primary tumor)	87.2 ± 48.3	157.8 ± 53.8
PDA (metastasis)	118.3 ± 61.8	144.7 ± 44.3

#10- Lymphocytic Esophagitis Revisited: Still a Histologic Disease with No Clinical Associations

Mark Ettel, Henry D. Appelman

Presented at: submitted and pending review for Digestive Disease Week in June, 2018
Manuscript: In preparation

Objectives Lymphocytic esophagitis (LE) is a histologic disease characterized by excess numbers of lymphocytes with no more than rare granulocytes in the squamous epithelium accompanied by spongiosis (a sign of injury) and basal cell hyperplasia (a sign of repair). In a retrospective case-controlled study we reported in 2008, we found no differences in clinical or endoscopic associations between LE patients and controls. Since then studies have reported associations between LE and Crohn's disease in children and between LE and primary esophageal motility disorders. We decided to perform the first prospective case-controlled study of LE to see if our original retrospective study findings still were valid.

Methods: We reviewed all adult esophageal biopsies collected from December 2016 through June 2017 at our institution excluding those with eosinophilic esophagitis, Barrett's mucosa and neoplasms. We screened the biopsies for findings of LE as defined above. For every case of LE, we selected two control patients randomly from among those patients found not to have LE. We recorded and compared endoscopic findings, symptoms, clinical diagnoses and demographic characteristics in both the patients with LE and controls.

Results: 437 patients underwent esophageal biopsy during the study period, of which 47 (10.8%) had LE. These were compared to a control group of 94 patients. Age (p=0.418) and gender (p=0.355) were no different between LE (median age 54 years; 70.2% women) and control groups (median age 51 years; 61.7% women). Endoscopic findings resembling those in eosinophilic esophagitis such as rings (p=0.436) and furrows (p=0.534) were no more likely to be seen in LE patients than control patients, and no other endoscopic associations were identified. There was a trend toward an increased prevalence of dysphagia (72.3% in LE vs. 55.3% in controls; p=0.067). There was no difference between LE and control patients in findings of dysmotility (14.9% in LE vs. 6.4% in controls; p=0.125). Other findings such as H. pylori gastritis (p=0.719), and allergic conditions (p=0.168) were no more likely to be found in LE compared to controls. There were not enough patients with Crohn's disease to test the association between that disease and LE.

Conclusions:
In this prospective case-controlled study we found no definite association between LE and any clinical disease or symptom in the adult population, identical findings to those in our retrospective study of 10 years ago. LE remains a histologic disease without a clear clinical association.

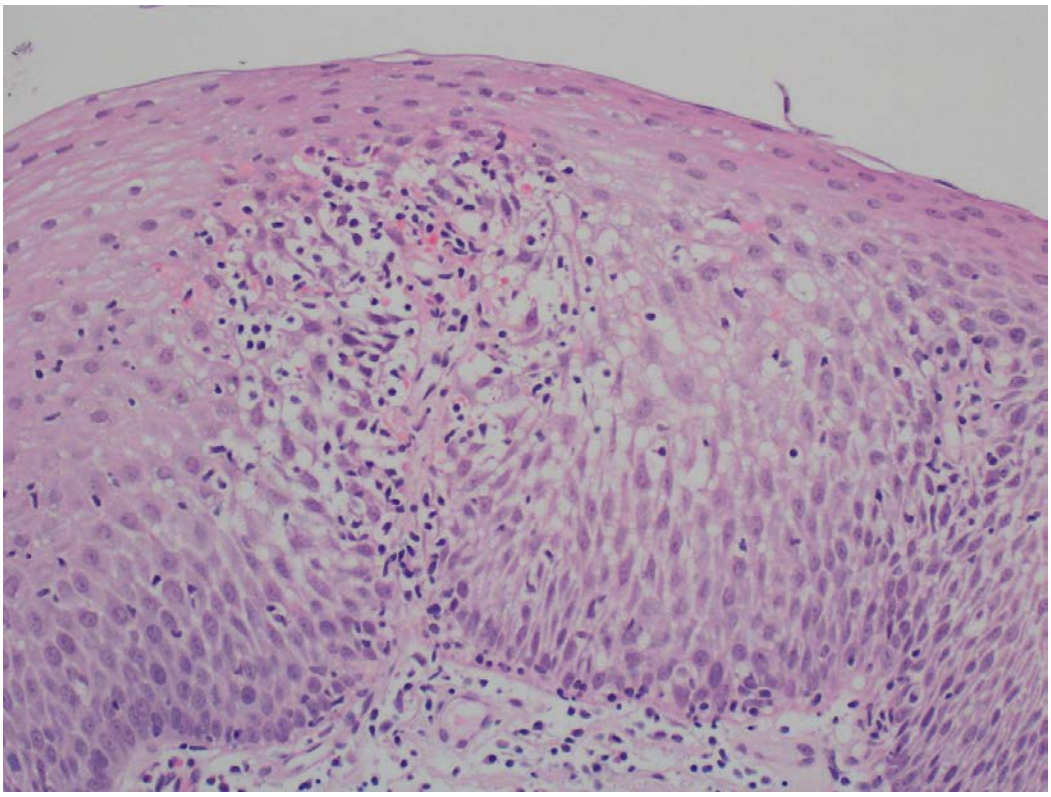

#11 - Opioid Use Trends in South East Michigan

Brittany R. Jullie, Bradley J. Kay, Thomas J. Sheppard

Funded by: Undergraduate Research Opportunity Program
Manuscript: In preparation

In recent years, there has been an increase in abuse of opioids among Americans, which can lead to addiction, increased tolerance, and overdoses[1]. One factor that could explain this is the increasing number of prescriptions for opioids written by physicians[1]. The aim of this study was to look at urine drug test results in the University of Michigan hospital system from January 2015 to June 2017 in order to assess opioid use trends among patients during this time period. The drug test results were analyzed in a spreadsheet format. The COUNTIF function in Microsoft Excel was used to count the occurrences of each type of drug and perform descriptive statistics. These occurrences were organized by class of drug and pie charts were made for each class showing which drugs were most common. Additionally, a table showing the overall prevalence of opioid use among this sample is being created. The results showed that the most common opioids used were hydrocodone, tramadol, and oxycodone. This information can be relayed to physicians and other medical practitioners in order to inform them of what drugs are commonly abused. However, there is not enough information to determine whether these opioids used were prescribed or not. An additional limitation is that drug assays are more sensitive to some drugs than others. In the future, data from other hospital systems can be included in this study, and eventually this will provide an estimate of the proportion of hospital patients using opioids.

[1]Compton, W. M., & Volkow, N. D. (2006, February). Major increases in opioid analgesic abuse in the United States: Concerns and strategies. *Drug and Alcohol Dependence*, *81*(2), 103-107.

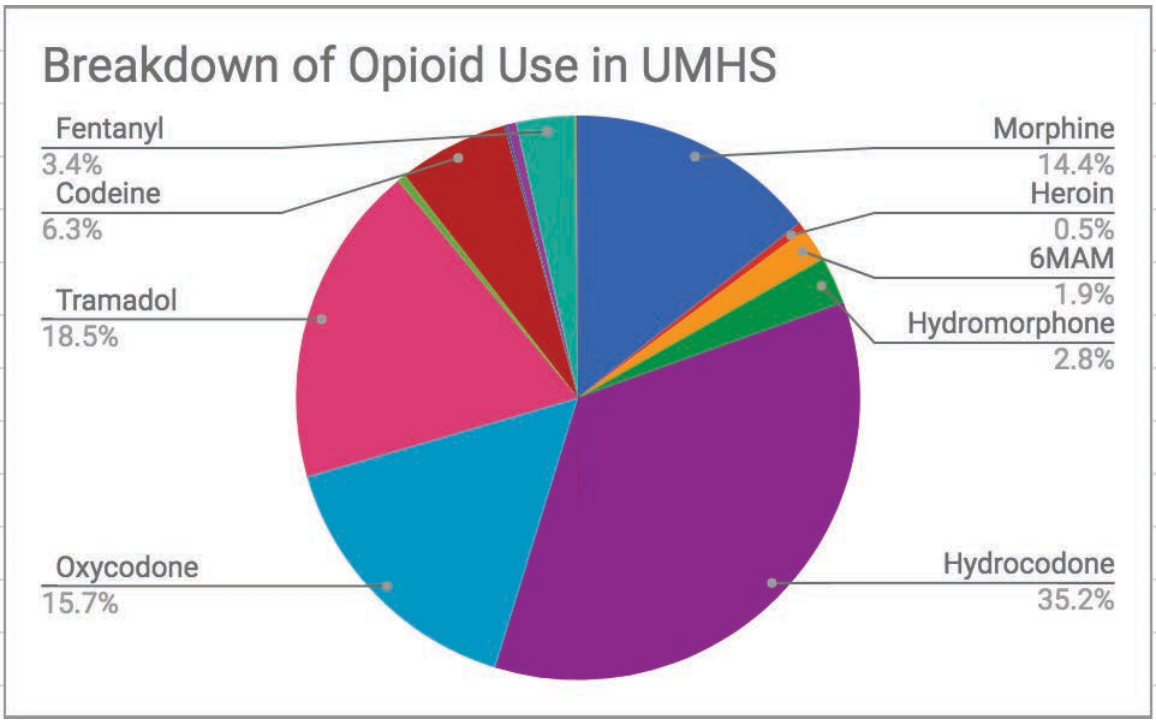

#12 - Morphologic and Clinical Review of 62 Renal Tumors in 30 Patients with Familial Kidney Cancer Syndromes

John Kennedy, Aaron Udager, Priya Kunju, Madelyn Lew, Arul Chinnaiyan, Scott Tomlins, Angela Wu, Rohit Mehra

Background: Most renal cell carcinomas (RCC) occur sporadically, although a small subset are associated with hereditary syndromes (HS). Due to the rarity of each individual HS, there are few comprehensive studies investigating the clinicopathologic features of these tumors. The present study is a retrospective review at our institution to further characterize the clinicopathologic spectrum of HS tumors.

Design: The medical record was searched for renal biopsies/resections of HS patients seen at a single large academic institution since 2000. The search yielded 62 renal biopsies/resections from 30 patients with HS, including Von-Hippel Lindau (VHL), Birt-Hogg-Dube (BHD), tuberous sclerosis (TS), hereditary leiomyomatosis and renal cell carcinoma (HLRCC), and succinate dehydrogenase deficiency (SD). Twenty-four patients with 41 tumor biopsies/resections were available for morphologic review.

Results: See table for summary of tumor type, stage, grade, and multifocality for each HS. Morphologic features for each HS are described below. VHL: 86% of resections (n=21) had cystic CCRCC and/or atypical clear cell lined cysts. 40% of patients (n=10) had tumorlets within benign renal parenchyma of at least one resection specimen. BHD: 25% of resection specimens (n=4) available for review showed background renal oncocytosis. TS: All resections (n=3) available for review demonstrated background cysts. Features of epithelioid AML and AML tumorlets were seen in 67% of cases (n=3). Clinical and pathologic data for patients with HLRCC and SD is being analyzed currently. Of all masses biopsied in HS patients (n=24), 8% of cases led to a new diagnosis of HS by molecular testing. Indications for biopsy in patients with a HS diagnosis included radiosurveillance of a renal mass (79%) and confirmation of successful radioablation treatment (8%). One biopsy on a patient without a HS diagnosis did not prompt testing, but later clinical information led to SD testing. Additional biopsy data and subsequent patient management is currently being analyzed.

Conclusions: Renal tumors associated with HS frequently have characteristic morphologies unique to each HS. Multifocality is common in both benign and malignant tumors of HS patients. Both VHL and BHD related-RCCs are identified at low stage (T1), most likely due to radiologic surveillance of HS patients. Renal biopsies rarely led to a new diagnosis of HS, but play an important role in the surveillance of renal masses in HS patients.

#13 - Targeted Genomic Profiling of Sinonasal Melanoma Reveals Novel Oncogenic Alterations, including Focal Very High Copy Number Gains of *KRAS* and *MET*

Zaid Mahdi, Komal R. Kunder, Jonathan B. McHugh, Rajiv M. Patel, Scott A.Tomlins, Aaron M. Udager

Presented at: Accepted for poster presentation at USCAP 2018
Funded by: AP Project Funding Committee
Manuscript: In preparation

Background: Malignant melanoma is an uncommon primary tumor of the sinonasal tract that often has a poor long-term clinical outcome. Conventional chemotherapy is typically ineffective for locally-advanced or metastatic sinonasal melanoma (SM), necessitating the development of novel targeted therapeutic approaches for these aggressive tumors. In this study, we utilized targeted next-generation DNA sequencing (DNAseq) to identify possible targetable oncogenic alterations in SM.

Design: SM from a single large academic institution between June 2013 and June 2017 were retrospectively identified, and representative formalin-fixed paraffin-embedded tissue was selected for targeted DNAseq using the Oncomine Comprehensive Assay and an Ion Torrent Proton sequencer. Somatic variants and copy number alterations (CNA) were identified via in-house bioinformatics pipelines, and prioritized alterations were nominated by manual curation using previously established criteria.

Results: 10 SM were available for the purposes of this study. Sequencing data was available for 9 tumors (90.0%) and demonstrated a total of 12 prioritized somatic variants (median per tumor = 1; range = 1-2), including oncogenic alterations in *NRAS* (*n* = 4), *BRAF* (*n* = 1), *KIT* (*n* = 1), and *HRAS* (*n* = 1); prioritized tumor suppressor mutations included *CDKN2A* (*n* = 1), *NF1* (*n* = 1), *ATM* (*n* = 1), *TET2* (*n* = 1), and *DDR2* (*n* = 1). All oncogenic somatic variants were mutually exclusive. A total of 44 CNA were identified (median per tumor = 5; range = 0-9). Recurrent CNA included *MYC* (gain; *n* = 5), *MCL1* (gain; *n* = 4), and *CDKN2A* (loss; *n* = 3), and the sole *KIT*-mutated tumor showed no CNA. Focal very high copy number gains of *KRAS* (22-fold; *n* = 1) and *MET* (25-fold; *n* = 1) were detected in two tumors without prioritized oncogenic somatic variants. Therefore, overall, all sequenced tumors harbored either an oncogenic somatic variant or focal very high copy number gain.

Conclusion: SM shows a very high rate of potentially targetable oncogenic alterations in growth factor signaling pathway genes, including frequent somatic mutations (77.8%) and occasional focal very high copy number gains (22.2%), providing a rational basis for therapeutic targeting of downstream MAPK/MEK activity in these aggressive tumors. Comprehensive genomic profiling with targeted DNAseq may be indicated for “triple-negative” SM without oncogenic *NRAS*, *KIT*, or *BRAF* mutations to identify other less common targetable oncogenic alterations.

#14 - Trends in Opioid Use In Washtenaw County

Brittany Jullie, Thomas Sheppard, Bradley Kay, Hema Ketha

Manuscript: In preparation

Background United States is the largest consumer of prescription opioids. Economic, social and healthcare burden of opioid over use is rising rapidly. Understanding trends in opioid use in large health systems can help shape policies that will be of immense value.
Objective: The study objective was to identify trends of specific drug use at the University of Michigan Health System (UMHS) through analysis of urine drug testing data.
Methods: Urine drug testing is performed at the UMHS primarily for monitoring compliance to controlled substance use and to support addiction treatment programs. The data from UMHS hospital system were considered representative of opioid and other drug use trends frequent in Washtenaw County.

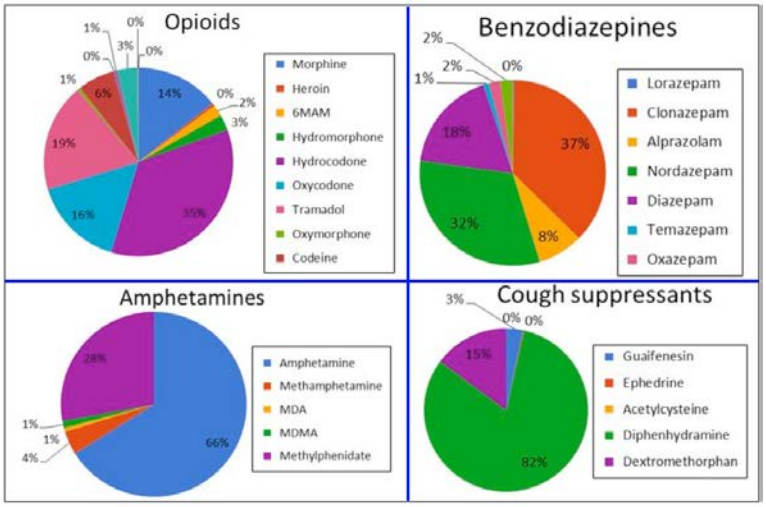

Drug Class	Count	% of Class	% of Total
Opioids	6729		
Morphine	965	14.34%	6.56%
Heroin	32	0.48%	0.22%
6MAM	130	1.93%	0.88%
Hydromorphone	185	2.75%	1.26%
Hydrocodone	2367	35.18%	16.09%
Oxycodone	1053	15.65%	7.16%
Tramadol	1250	18.58%	8.50%
Oxymorphone	33	0.49%	0.22%
Codeine	426	6.33%	2.90%
Dihydrocodeine	11	0.16%	0.07%
Naloxone	35	0.52%	0.24%
Fentanyl	232	3.45%	1.58%
Tapentadol	5	0.07%	0.03%
Meperidine	5	0.07%	0.03%
Amphetamines	876		
Amphetamine	579	66.10%	3.94%
Methamphetamine	36	4.11%	0.24%
MDA	6	0.68%	0.04%
MDMA	11	1.26%	0.07%
Methylphenidate	244	27.85%	1.66%
Selegiline	0	0.00%	0.00%
Barbiturates	536		
Secobarbital	0	0.00%	0.00%
Phenobarbital	275	51.31%	1.87%
Primidone	43	8.02%	0.29%
Butalbital	218	40.67%	1.48%
Benzodiazepines	497		
Lorazepam	1	0.20%	0.01%
Clonazepam	189	38.03%	1.28%
Alprazolam	40	8.05%	0.27%
Nordazepam	162	32.60%	1.10%
Diazepam	90	18.11%	0.61%
Temazepam	5	1.01%	0.03%
Oxazepam	10	2.01%	0.07%
Clobazam	11	2.21%	0.07%
Cocaine	527		
Cocaine	361	68.50%	2.45%
Benzoylecoginine	24	4.55%	0.16%
Cocaethylene	10	1.90%	0.07%
Methylecoginine	132	25.05%	0.90%

Drug Class	Count	% of Class	% of Total
Designer Compounds			
Antidepressants	4373		
Fluoxetine	360	8.23%	2.45%
Citalopram	1064	24.33%	7.23%
Sertraline	703	16.08%	4.78%
Bupropion	710	16.24%	4.83%
Mirtazapine	366	8.37%	2.49%
Nortriptyline	481	11.00%	3.27%
Venlafaxine	586	13.40%	3.98%
Paroxetine	61	1.39%	0.41%
Doxepin	42	0.96%	0.29%
Cough suppressants		2421	
Guaifenesin	81	3.35%	0.55%
Ephedrine	4	0.17%	0.03%
Acetylcysteine	0	0.00%	0.00%
Diphenhydramine	1978	81.70%	13.45%
Dextromethorphan	358	14.79%	2.43%
Antipsychotics	1412		
Clotiapine	0	0.00%	0.00%
Clozapine	15	1.06%	0.10%
Quetiapine	662	46.88%	4.50%
Trazodone	583	41.29%	3.96%
Olanzapine	152	10.76%	1.03%
Gabapentin	1429		9.72%
OTC Drugs	5145		
Acetaminophen	3147	61.17%	21.40%
Pseudoephedrine	153	2.97%	1.04%
Ibuprofen	1190	23.13%	8.09%
Naproxen	332	6.45%	2.26%
Doxylamine	323	6.28%	2.20%
Anticonvulsants	1064		
Topiramate	393	36.94%	2.67%
Levetiracetam	293	27.54%	1.99%
Phenytoin	61	5.73%	0.41%
Lamotrigine	317	29.79%	2.16%

We analyzed urine drug testing result data from all patients being tested at UMHS from January 2015 to July 2016. Samples that had the drug screen by gas chromatography mass spectrometry (GC-MS) performed at the UMHS Toxicology Laboratory were included in the study. Nicotine, caffeine alone being present was not considered as a positive GC-MS result. Samples with negative results (no drugs identified other than nicotine and caffeine) were excluded. Results from GCMS testing for all the included samples were transcribed into Microsoft Excel worksheets. Sample results were analyzed using Microsoft Excel to identify the most common drug used in each of the following classes: opioids, stimulants, benzodiazepines. Other commonly occurring drugs from over the counter cough suppressants, anti-psychotics, anticonvulsants and antidepressants were also identified.

Results: Urine drug testing results from a total of N=14709 samples tested by GC-MS assay in the study period (1st January 2015-30th June 2016) were included in the analysis. 6729 samples (46%) were confirmed positive for one or more opioids. The most common opioid identified amongst UMHS patients being tested using urine drug test was hydrocodone (2367/6729). Oxycodone (1053/6729) and tramadol (1250/6729) were the next most used opioids. Benzodiazepines were detected only 497 times most likely due to (well known) poor diagnostic sensitivity of GC-MS to detect this drug class. Amongst benzodiazepines detected, clonazepam was the preferred drug. Table 1 shows the number of occurrence of each drug by drug class. Figure 1 shows pie charts for each drug class showing the most commonly identified drug in each class. Pie charts for opioids, benzodiazepines, amphetamines and OTC cough suppressants are shown. Dextromethorphan and diphenhydramine were the most commonly used cough suppressants.

Conclusions: The most common drugs identified in each class are most indicative of the common drug overused and likely abused too. Of note, policies for cautious prescribing and improved monitoring of hydrocodone, oxycodone and tramadol may be of institutional value.

Further Work: Correlation of GCMS data with another testing modality (immunoassay screen) on samples for which data from both tests are available in the same time frame are being studied. Any new designer drugs that have been identified in UMHS will be identified. This step can help us develop optimum testing strategies for the major drugs used and/or abused at UMHS.

#15 - Utility of Reflexing Suspicious Beta Region Findings on Capillary Serum Protein Electrophoresis to Immunofixation for Detecting Monoclonal Gammopathies

Amanda L. Kitson, Donald A. Giacherio, David F. Keren

Manuscript: In preparation, beta1 and beta2 region re-analysis

Background Serum protein electrophoresis (SPEP) is a technique in which abnormal serum proteins can be detected based upon the migration patterns of the proteins, aiding in the diagnosis of diseases such as multiple myeloma. Immunofixation (IFE) can be performed subsequently to identify and characterize the isotype of a monoclonal immunoglobulin. Although much work has been done to determine when reflex IFE should be performed, there is lack of clarity of when this should be implemented for abnormalities within the beta region. Currently, in most laboratories, including our own, the beta region, which consists primarily of transferrin (beta1) and C3 (beta2), is measured in aggregate. Our laboratory performs reflex IFE in cases where there is suspicion of a beta region monoclonal protein (M-protein). The present study evaluates the utility of our reflex strategy in detecting M-proteins.

Methods: A retrospective review was conducted of SPEP cases performed at Michigan Medicine from June 2013 to June 2017. Capillary electrophoresis using the Sebia Capillarys was the routine screening method during this time period. Although the capillary electrophoresis method used provides a crisp separation of the beta1 and beta2 bands which could allow separate measurements, our laboratory conforms with the more traditional use of a 5 zone measurement (albumin, alpha1, alpha2, beta and gamma). Cases were selected based on the use of a searchable comment “possible restriction in the beta region” (PRB), used to denote a suspicious process within the beta region. This comment automatically reflexed the specimen to an IFE. The PRB comment was used in three situations: the presence of a suspicious spike within the beta region, a beta1-beta2 bridge, or an increase in the total beta region without an obvious explanation, such as the prominent beta-gamma bridge typically seen in cases of cirrhosis, indicating a polyclonal increase in IgA. The search revealed a total of 2,134 cases. For patients with multiple samples, only the initial sample showing a PRB comment was included. In addition, one case was excluded due to concern of a mislabel. After removing these cases, 1,923 cases remained for evaluation. For each patient, the beta region protein concentration was recorded, as well as the presence or absence of an M-protein and its isotype as identified by IFE. For cases where the IFE did not identify an M-protein, the presence of a polyclonal increase in immunoglobulins was recorded.

Due to suggestions from recent literature to report beta1 and beta2 regions separately when the electrophoretic method had sufficient resolution to warrant this, reference ranges for the beta1 and beta2 regions were constructed using 31 normal patient samples that were previously used to establish our current reference intervals in 2014. The reference ranges were determined using the mean protein concentration ± 2 standard deviations.

Results: Of the total 1,923 cases with possible beta region restriction, 287 had an M-protein detected on IFE (14.9%) and 1,632 had no M-protein identified (84.9%). Two cases showed a possible faint restriction and two cases were reported to show a tiny clonal restriction.

Of the 287 cases with a definitive M-protein demonstrated on IFE, IgA kappa was the most common isotype (79/287, 27.5%), with IgA lambda being the second most common (66/287, 23.0%). Other reported M-protein isotypes were IgG kappa (53/287, 18.5%), IgM kappa (37/287, 12.9%), IgG lambda (27/287, 9.4%), IgM lambda (12/287, 4.2%), lambda free light chain (19/287, 6.6%), kappa free light chain (10/287, 3.5%), and IgD lambda (1/287, 0.35%). Of note, 17 cases had multiple M-protein isotypes present.

Analysis of the normal patient samples resulted in a mean beta1 protein concentration of 0.46 g/dL, corresponding to a reference range of 0.31-0.61 g/dL, and a mean beta2 protein concentration of 0.40 g/dL, corresponding to a reference range of 0.24-0.57 g/dL.

Conclusions: Our current SPEP method of reflexing samples with suspicious beta region findings revealed the presence of an M-protein in 14.9% of the cases reflexed to IFE. Nonetheless, because almost 85% (false positives) of our reflexed cases failed to detect an M-protein, we wish to further interrogate our cases to fine tune the criteria used in reflexing samples to IFE. One recent and one older study in the literature have suggested that separate measurement of the beta1 and beta2 regions may improve detection of beta region M-proteins. The reference ranges for beta1 and beta2 that were constructed using normal patient samples are in agreement with a recent report that also used the Sebia Capillarys. Using our newly determined beta1 and beta2 region reference intervals, further study will be performed to see if this improves our precision in selecting cases to reflex for IFE.

#16 - Immediate Bedside Adequacy Assessment of Bone Marrow Core Biopsies: Early Identification of Sub-Optimal Evaluations Through Evaluable Marrow Length and Inter-Trabecular Areas by X-Ray Imaging

Amanda L. Kitson, Srikanth Ragothaman, Rajan Dewar

Manuscript:: USCAP

Background Adequate bone marrow (BM) evaluation is crucial to the diagnosis of hematolymphoid disorders, providing information on the overall cellularity, lineage proportion and morphology, and allowing for immunohistochemical staining. The 2008 World Health Organization (WHO) defines an adequate BM core biopsy as 1.5 cm in length with at least 10 morphologically preserved inter-trabecular areas (ITA). However, gross examination of the core biopsy can be misleading due to attached clot, thick periosteum and bone, or tangential biopsies, resulting in a long biopsy fragment without adequate evaluable marrow or ITAs by microscopy. Suboptimal BM biopsies hinder appropriate diagnosis, delay patient care, and may require the patient to undergo additional BM biopsies. Image analysis via a cabinet x-ray system can be utilized as a point-of-care tool to assess the amount of evaluable marrow and ensure an adequate core biopsy at the bedside, permitting the collection of additional tissue at time of the procedure if necessary.

Design: 53 consecutively obtained BM biopsies were obtained and analyzed with a cabinet x-ray system (Faxitron) soon after biopsy, then subjected to routine histology and processing. High resolution images of the core biopsy were obtained (Fig. 1). Length of the biopsies and number of ITAs were calculated from the x-ray images. Gross measurement of biopsy length and microscopic assessment of evaluable marrow were compared to the measurements obtained by x-ray imaging. Adequate BM biopsies were defined as at least 1.5 cm of evaluable marrow with at least 10 ITAs.

Results: Only 13/53 core biopsies exceeded the WHO standard of 1.5 cm by microscopy, while 34/53 were grossly estimated to be >1.5 cm (mean overestimation of 0.43 cm/biopsy by gross measurement, Fig. 2). There was general concordance between the number of ITAs and length of core biopsies. 10/53 biopsies were <1 cm. Utilizing x-ray image measurements, core biopsy fragment length was shown to be in great agreement with microscopic estimation of BM core biopsy length and number of ITAs. X-ray imaging readily identified clot sections (non-radiopaque), sclerotic cortical bone (absence of trabeculae), and periosteum (soft tissue shadow) in all 10 sub-1 cm biopsies.

Conclusion: We conclude that core biopsy length and number of ITAs can easily be estimated using bedside point-of-care x-ray analysis to ensure adequate BM evaluations. We propose the routine use of this technology for immediate assessment of BM core biopsies.

#17 - A Case Series of Incidental Maternal Endometrial Polyp Within the Placenta (MEPP)

Emily R McMullen, Richard W Lieberman

Manuscript: In preparation

Background: Endometrial polyps are common lesions that are found within the uterine cavity of women, and can be asymptomatic, associated with abnormal uterine bleeding or infertility. As common as endometrial polyps are, their presence as an incidental finding with in the placenta has not been previously described. Our institution has accumulated three cases of term placentas with an incidental finding of a retained endometrial polyp, also known as the maternal endometrial polyp within the placenta (MEPP). MEPPs should not to be confused with placental polyps, a radiologic term used to describe retained placental tissue. We report three cases of maternal endometrial polyps incorporated into each placenta over the course of gestation and identified during the gross placental evaluation.

Design: We searched our institutional archives for the terms “placenta” and “endometrial polyp” from 1997 to 2016 and yielded 3 cases. All H&E slides and gross photos were re-reviewed with special attention to the histopathology and relevant clinical history.

Results: All three placental cases were submitted for histologic review under the 1996 CAP guidelines. The maternal ages ranged from 29-37, and all three cases delivered a healthy term infant. Grossly, all cases showed a well-circumscribed white nodule associated within the placental specimen. In each case, the nodules were located in different locations including the disk parenchyma, amniotic membranes, and retroplacental maternal-fetal interface. Based on the gross examination, the differential diagnosis included a placental infarct, an organizing intervillous thrombus, or a chorangioma. Histologically, the nodules were endometrial polyps with prominent decidualized stroma, thick vascular bundles, and endometrial glands with gestational changes, consistent with MEPPs. No pregnancy complications occurred in association with the MEPPs.

Conclusion: We describe three cases of incidental MEPP (maternal endometrial polyps within a placenta). Incidental MEPPs should be distinguished from the previously described “placental polyp” due to the clinical implications of this term. Placental polyps are chorionic remnants that are retained within the uterine cavity and can cause post-delivery uterine bleeding and elevations in beta-HCG, and thus require removal. MEPPs are histologically maternal in origin becoming associated with the placenta over the course of gestation. In our case series, these lesions were benign and incidental with no associated clinical outcomes.

#18 - Clinicopathologic Features and Calcium Deposition Patterns in Calciphylaxis: Comparison with Peripheral Artery Disease, Chronic Stasis, and Thrombotic Vasculopathy

Emily R McMullen, Lori Lowe, Douglas R Fullen, May P Chan

Manuscript: In preparation

Background: Diagnosis of calciphylaxis is crucial in prompting timely treatment, yet its distinction from other vascular diseases can be challenging. While vascular calcification and thrombosis are histopathologic hallmarks of calciphylaxis, the incidence and patterns of these features in other vascular diseases have not been well characterized. In particular, it remains unclear whether stippled calcium deposits identified on von Kossa (VK) stain only are specific for calciphylaxis, or may be seen in other conditions as well.

Design: Cases of calciphylaxis (n=24), peripheral artery disease (gangrene and uninvolved skin at amputation margin, n=21 each), chronic stasis (n=22), and thrombotic vasculopathy (n=19) were retrospectively reviewed. VK stain was performed and examined in all cases.

Results: Clinical and histopathologic findings are summarized in the Table. Patients with calciphylaxis were much more likely to be on hemodialysis ($p<0.0001$) and have documented hypercalcemia, hyperphosphatemia, and/or hyperparathyroidism ($p<0.0001$). Concentric calcification of subcutaneous small vessels appreciable on H&E is relatively specific for calciphylaxis, although sensitivity was limited (50%). VK allowed for detection of stippled calcium deposits otherwise not appreciable on H&E, but the specificity of such deposits was low. In fact, stippled calcium deposits in subcutaneous small vessels were more common in clinically normal skin (amputation margin) of patients with severe peripheral artery disease (86%) than in calciphylaxis (46%). Specificity of stippled calcium in subcutaneous small vessels (identified on VK only) improved when concomitant thrombosis was present. Calcium deposits in medium-sized vessels, eccrine gland basement membranes, and elastic fibers had minimal specificity.

Table 1	Calciphylaxis (n=24*)	Gangrene (n=21)	Amputation margin (n=21)	Chronic Stasis (n=22**)	Thrombotic vasculopathy (n=19)
Clinical					
Mean age	60	68		59	55
Sex (male:female)	3:20	13:8		3:18	11:8
Diabetes	11 (48%)	11 (52%)		6 (29%)	4 (21%)
Chronic kidney disease	16 (70%)	6 (29%)		6 (29%)	8 (42%)
Hemodialysis	10 (43%)	0		0	0
Peripheral artery disease	4 (17%)	21 (100%)		2 (10%)	2 (11%)
Elevated calcium, phosphate, or parathyroid hormone	20 (83%)	4 (19%)		3 (14%)	1 (5%)
Histopathology					
Thrombosis in subcutaneous small vessels	22 (92%)	14 (67%)	0	4 (18%)	5 (26%)
Calcium in subcutaneous small vessels:					
- Identified on H&E	12 (50%)	3 (14%)	0	0	0
-Identified on VK	23 (96%)	12 (57%)	18 (86%)	5 (23%)	1 (5%)
-Identified on VK only	11 (46%)	9 (43%)	18 (86%)	5 (23%)	1 (5%)
Calcium and thrombosis in subcutaneous small vessels:					
- Ca identified on H&E	10 (42%)	2 (10%)	0	0	0
- Ca identified on VK	21 (88%)	9 (43%)	0	1 (5%)	0
- Ca identified on VK only	11 (46%)	7 (33%)	0	1 (5%)	0
Calcium in medium vessels:					
- Ca identified on H&E	17 (71%)	4 (19%)	6 (29%)	1 (5%)	0
- Ca identified on VK	20 (83%)	8 (38%)	19 (90%)	4 (18%)	3 (16%)
- Ca identified on VK only	3 (13%)	4 (19%)	13 (62%)	3 (14%)	3 (16%)
Calcium in eccrine gland basement membranes (VK)	13 (54%)	2 (10%)	7 (33%)	1 (5%)	3 (16%)
Calcium in elastic fibers (VK)	14 (58%)	3 (14%)	4 (19%)	10 (45%)	0
Extravascular calcification (H&E)	8 (33%)	6 (29%)	6 (29%)	6 (27%)	0
Neutrophils in fat	14 (58%)	19 (90%)	1 (5%)	4 (18%)	8 (42%)
Fat necrosis	23 (96%)	21 (100%)	7 (33%)	21 (95%)	5 (26%)
Septal fibrosis	18 (75%)	21 (100%)	7 (33%)	21 (95%)	3 (16%)

* 24 Biopsies from 23 patients. ** 22 Biopsies from 21 patients.

Conclusion: Despite limited sensitivity, concentric calcification of subcutaneous small vessels appreciable on H&E is relatively specific and sufficient to favor a diagnosis of calciphylaxis. VK is useful in enhancing detection of calcium and avoiding false negative diagnosis based on H&E only. When stippled calcium deposits are identified on VK only, concomitant thrombosis of the subcutaneous small vessels is necessary to support a diagnosis of calciphylaxis in the correct clinical setting. As none of the examined histopathologic features are definitively diagnostic of calciphylaxis, correlation with clinical and laboratory findings remains imperative.

#19 - Intraepidermal Merkel Cell Carcinoma Mimicking Epidermotropic T-cells in a Sezary Syndrome Patient

Nicholas Zoumberos, Trilokraj Tejasvi, Kelly Harms, Douglas Fullen, Paul Harms

Presented at: Presented at ASDP 2017
Manuscript: In preparation

Merkel cell carcinoma (MCC) is a rare, aggressive cutaneous neuroendocrine carcinoma with increased prevalence in patients with immunosuppression or B-cell chronic lymphocytic leukemia. To our knowledge, an association with cutaneous T-cell lymphoma (CTCL) has not been previously described. Although a subset of MCC tumors display epidermal involvement, purely intraepidermal MCC is exceedingly rare. In this case we present a Caucasian female in her 70s who presented for management of previously diagnosed Sezary syndrome. A biopsy of an erythematous patch with a fine scale revealed two distinct abnormal cell populations. The first population consisted of hyperchromatic lymphocytes located in the superficial dermis with minor epidermotropic spread into the epidermis; this population of cells expressed CD3 and CD4 with diminished CD7 expression. The second population of cells consisted of intraepidermal clusters of larger atypical cells that expressed synaptophysin, neurofilament, and CK20, and were negative for lymphoid markers including CD3, CD4, TCFBR1, and CD45. The combination of findings was consistent with intraepidermal MCC in a background of CTCL. Excision demonstrated residual intraepidermal MCC without dermal involvement. The patient had no evidence of recurrent MCC after five months of follow-up. Our case demonstrates that MCC may rarely occur in the setting of T-cell lymphoma, and may mimic epidermotropic T-cells in this context.

#20 - Reproducibility of Pattern-Based Classification for Endocervical Adenocarcinoma - An Institutional Experience

Sarah Rooney, Richard Lieberman

Funded by: AP Project Funding Committee
Manuscript: In preparation

Background: A pattern-based classification system for invasive endocervical adenocarcinoma has been shown to be predictive of nodal metastases and recurrence and can spare patients with no risk of recurrence after complete resection, the morbidities of further treatment. However, the reproducibility of this pattern classification system has had mixed results. We sought to determine if the pattern classification system could be applied to our patient population and pathology group.

Design: We retrospectively reviewed available histologic and clinical data in patients diagnosed with invasive endocervical adenocarcinoma at the University of Michigan between 1990 through 2015. We then assigned pattern of invasion based on the recently proposed classification system by Diz De Vivar et al. and performed sensitive HPV PCR testing (Multiplex PCR) on all cases to determine HPV-type.

Results: We assigned pattern of invasion to 54 of 69 invasive adenocarcinomas. We had 7 cases of pattern A (13%), 28 cases of pattern B (52%), and 18 cases of pattern C (33%), and 1 case of mixed pattern B and C (2%). None of the patients with pattern A invasion recurred (average follow up time 8 years). Two patients with pattern B invasion recurred both at 3 years. Four patients with pattern C recurred at 1, 2, 3 and 6 years.

Conclusion: Our data support the prognostic value of pattern classification. Based on our cohort, there is no risk of recurrence in pattern A invasive endocervical adenocarcinoma. There is a trend for higher risk of invasion with increasing pattern classification from A to C. The pattern classification system is reproducible within our pathology group.

#21 - Cervical Glandular Neoplasia in the United States: Increasing Prevalence and Inadequate Screening Practices

Sarah Rooney, Christine Goudsmit, Heather Walline, Tom Carey, Richard Lieberman

Funded by: AP Project Funding Committee
Manuscript: In preparation

Background: Since the 1970s cervical glandular neoplasia (CGN) (encompassing adenocarcinoma in situ (AIS) and adenocarcinoma) has increased in prevalence in absolute, not just relative, terms when compared to squamous cell carcinoma. CGN can present a diagnostic challenge because current screening methods for cervical neoplasia are most appropriate for squamous lesions. With increasing prevalence of CGN, appropriate screening protocols need to be determined.

There is an abundance of literature on HPV-related squamous neoplasia but very limited regarding glandular lesions. A recently published collaborative study by 12 European groups found variations in HPV prevalence and ADC type-distribution by country. However, we were unable to find publications of large CGN cohorts from the United States.

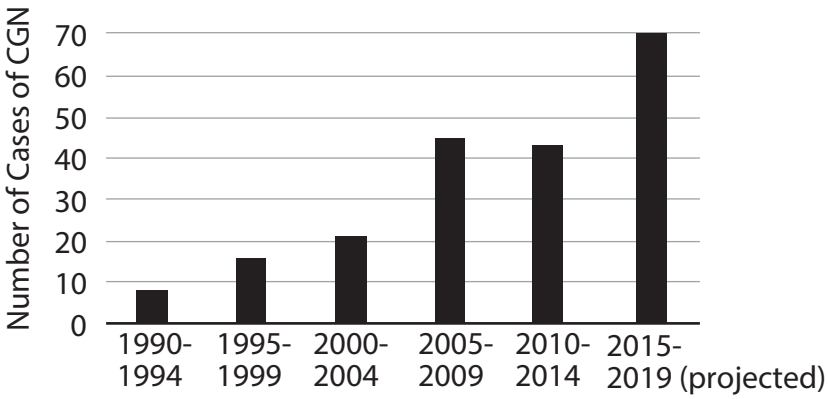

Figure 1. Increasing Prevalence of CGN from 1990 to 2015

Design: We retrospectively reviewed available cytology, human papilloma virus (HPV), and histologic, and clinical data in patients diagnosed with adenocarcinoma in situ (AIS) and adenocarcinoma at the University of Michigan between 1990 through 2015. We then performed sensitive HPV PCR testing (Multiplex PCR) on all cases to determine HPV-type.

Results: The prevalence of CGN at our institution has increased 5-fold since 1990 (Figure 1).

Table 1. HPV Type-specific prevalence in HPV-positive cases

	All Infections (Single or Multiple)		
	TOTAL (n=116)	AIS (n=47)	Invasive (n=69)
HPV16	72 (62.1%)	23 (48.9%)	49 (71.0%)
HPV 18	31 (26.7%)	17 (36.2%)	14 (20.3%)
HPV 33	1 (0.9%)	-	1 (1.4%)
HPV 45	6 (5.2%)	3 (6.4%)	3 (4.3%)
HPV 52	1 (0.9%)	1 (2.1%)	-
HPV 56	2 (1.7%)	2 (4.3%)	-
HPV 59	1 (0.9%)	1 (2.1%)	-
HPV 66	2 (1.7%)	-	2 (2.9%)

Of the 147 cases of glandular neoplasia, 116 were found to have HPV infection in the distribution seen in Table 1. Seventeen cases were negative due to low volume of DNA, 11 cases were presumed false negatives based on histologic review, 9 cases were negative due to a histology not associated with HPV infection.

Table 2. Molecular and cytology results at the time of screening prior to tissue diagnosis of glandular neoplasia

	Molecular screening results				
Cytology	HPV16 (n=5)	HPV18 (n=7)	HR HPV (n=34)	Equivocal (n=2)	Negative (n=1)
AGUS, NOS		1	9		
AGUS, FN	1	1	3	1	
AdenoCA			3		
ASCUS	1	2	11		1
LSIL			1		
HSIL			5	1	
Negative	4	3	2		

Fifty cases had concurrent molecular and cytology preceding tissue diagnosis of glandular neoplasia (Table 2). 41/50 cases detected cytologic atypia, either squamous and/or glandular (sensitivity of cytology alone 82%). Of the nine cases with negative cytology, on biopsy five had only glandular disease and four had both glandular and squamous disease. 1/50 cases was negative for HPV DNA (sensitivity of molecular alone - 98%). The one case with a negative molecular study was read on cytology as ASCUS and on biopsy this case had both glandular and squamous disease. The sensitivity of combined molecular and cytology was 100%.

Conclusion: The prevalence of CGN has increased significantly since 1990. Pap smear alone is an insensitive method of screening for glandular neoplasia and should be accompanied by molecular testing. HPV infection accounts for at least 80% of glandular neoplasia and should be incorporated into first line cervical screening.

#22 - Clinicopathologic Characteristics of Patients Undergoing Radical Prostatectomy (RP) with High-Risk (PI-RADS 5) Lesions by Prostate Multiparametric Magnetic Resonance Imaging (mpMRI)

Tanmay S. Shah, Aaron M. Udager, Rohit Mehra, Madelyn Lew, Scott A. Tomlins, Angela J. Wu, Matthew S. Davenport, Jeffrey S. Montgomery, L. Priya Kunju

Presented at: Accepted for presentation at USCAP 2018
Manuscript: In preparation

Background: mpMRI utilizes the PI-RADS v2 system to detect clinically significant [Grade Group (GG) 2 or higher] prostate cancer (PCa), with PI-RADS 5 lesions typically corresponding to high-risk disease. Our prior prostate biopsy (PBx) study showed that GG2 or higher PCa is detected in 79% of PI-RADS 5 lesions. Here, we analyzed clinicopathologic characteristics of RP specimens in patients with PI-RADS 5 lesions.
Design: All RP patients with ≥1 PI-RADS 5 lesion(s) on mpMRI between 1/1/15-6/30/16 at a large academic institution were retrospectively identified. All available cases were re-reviewed to assess stage and index tumor nodule parameters, including: location, size, GS, %Gleason pattern (GP) 4, and presence of cribriform architecture. Correlation between RP and mpMRI and PBx results was assessed.
Results: Of 199 patients with ≥1 PI-RADS 5 lesions, 120 underwent PBx and 68 underwent RP. Of 54 patients available for review (Table 1), one showed GG1, while the rest showed GG2 or higher (median %GP4=40). There was very high concordance (*n*=52; 96%) and moderate positive correlation (*P*<0.0001) between location and size of the index tumor nodule and the PI-RADS 5 lesion, respectively. The majority (*n*=30; 56%) of tumors were pT3a or higher; there was moderate to strong positive correlation for extraprostatic extension (EPE) and seminal vesicle invasion (SVI) (*P*<0.0001). The sensitivity of prostate mpMRI for detecting EPE or SVI was relatively low (<65%) and specificity was 89% and 100%, respectively. The majority (*n*=30; 56%) of index tumor nodules showed cribriform architecture, including 11 (20%) cribriform-predominant tumors (defined as >50% of tumor volume). The %GP4 in RP demonstrated strong positive correlation with highest %GP4 in prior PBx (*P*<0.0001). Overall, half of tumors demonstrated concordance between RP and PBx highest GG, with 16 (30%) showing GG upgrade (including 7/8 GG1 on PBx) and 11 (20%) showing GG downgrade; while only one clinically-significant upgrade (>1 GG) was identified, 7 tumors showed novel GP5 at RP (minor tertiary pattern in all but one case).

Table 1

RP	n = 54
Age	Median = 64 (range = 46-75)
Grade Group	GG 1: 2%
	GG 2: 44%
	GG2 with tertiary 5: 9%
	GG3: 20%
	GG3 with tertiary 5: 11%
	GG4: 4%
	GG5: 9%
Size of index nodule (cm)	Median = 2.6 (range = 0.8-4.3)
% GP4 (n=53)	Median = 40 (range = 10-100)
Presence of cribriform architecture in index nodule	56%
Cribriform-predominant index nodule (n=30)	20%
Anterior-dominant index nodule	38%
Multifocality	77%
EPE	57%
SVI	17%

Conclusion: The vast majority (98%) of patients with PI-RADS 5 lesions on mpMRI who undergo RP have clinically-significant PCa, with cribriform architecture present in more than 50% cases and 20% being cribriform-predominant. Significant moderate to strong positive correlation with several standard pathologic RP variables and mpMRI is observed. %GP4 on prior PBx is strongly correlated with %GP4 in the RP index tumor nodule.

#23 - Lymphoproliferative Disorders in Patients with Crohn's Disease

Yulei Shen, Scott R Owens, Sarah M. Choi, Lauren B Smith

Manuscript: In preparation

Crohn's disease (CD) is a form of chronic idiopathic inflammatory bowel disease (IBD) estimated to affect up to 700,000 Americans. It is often treated with immunosuppression. IBD patients, especially children and adolescents, on thiopurines and antitumor necrosis factor (anti-TNF) agents are thought to be at increased risk for lymphoproliferative disorders (LPD).

The database of the Department of Pathology was searched at our institution from June 2014-August 2017 in order to identify patients (both consultation and in-house) with a diagnosis of CD and lymphoproliferative disorders.

Nine patients with CD were identified. The patients had a median age of 59 years (range 22-72 years) and included five men and four women. Sites of involvement included colon (2), small intestine (1), stomach (1), liver (2), lymph node (1), adenoid (1), and skin (2). The moprhologic subtypes of the lymphoproliferative disorders included mycosis fungoides (MF) in two patients (one CD8 positive), peripheral T-cell lymphoma, NOS, diffuse large B-cell lymphoma (DLBCL) in two patients, EBV positive mucocutaneous ulcer (MCU), MALT lymphoma, T-cell histiocyte-rich large B-cell lymphoma (THRLBCL), and chronic lymphocytic leukemia/small lymphocytic lymphoma (CLL/SLL). One patient had two types of lymphoma (DLBCL and MF). Data on therapy was available for 6/9 patients. Therapies included infliximab (3 patients), adalimumab (3 patients), methotrexate (1 patient), azathioprine (1 patient), and mesalamine (1 patient). EBER (in situ hybridization for Epstein-Barr virus) was performed in 6/9 patients and two cases were positive. See table for summary of results.

Age (years)	Sex	Site	Morphologic Diagnosis	Medications	EBER
42	M	Rectosigmoid colon	MALT	Unknown	No done
72	F	Small intestine	EBV + MCU	Infliximab, adalimumab	+
24	M	Liver	THRLBCL	Infliximab	-
70	F	Skin	MF, CD8 positive	Unknown	Not done
45	M	Liver	HSTCL	Unknown	-
22	M	Adenoid	DLBCL, non-GCB	Adalimumab, methotrexate	+
59	M	Stomach	PTCL, NOS	Infliximab, adalimumab, azathioprine	-
68	F	Right axillary lymph node	CLL/SLL	No therapy	Not done
62	F	Colon, transverse & sigmoid Skin	DLBCL, non-GCB MF	Mesalamine	- in DLBCL Not done in MF

A variety of lymphoproliferative disorders can be seen in patients with CD, as demonstrated in this small series. Both T-cell and B-cell lymphoproliferative disorders were present. Only a subset of patients were postive for EBER. Extranodal sites were frequent, with the gastrointestinal tract being involved in 6/9 patients. If we exclude the patient with nodal disease who had CLL/SLL, which could easily be unrelated to CD (the patient was on no therapy), the number of patients with GI tract involvement is 6/8. A subset of patients was on immunosuppressive therapy, with some having a history of use of more than one agent. This small pilot study suggest that patients with CD can have a variety of LPDs and presentation in the GI tract is common.

#24 - Detection of *MDM2* Overexpression by RNA In Situ Hybridization (RNA-ISH) in Liposarcomas

Reena Singh, Lisha Wang, Dafydd G. Thomas, Jonathan B. McHugh, David R. Lucas, Aaron M. Udager, Rohit Mehra, Rajiv M. Patel

Presented at: Accepted for presentation at USCAP 2018
Funded by: National Cancer Institute SARC Sarcoma SPORE(U54 CA168512)
Manuscript: In preparation

Background: Detection of MDM2 amplification by fluorescence in situ hybridization (FISH) or MDM2 overexpression by immunohistochemistry (IHC) aids in distinguishing atypical lipomatous tumor/well-differentiated liposarcoma (ALT/WDLPS) and dedifferentiated liposarcoma (DDLPS) from their differential diagnostic considerations. FISH is highly sensitive but expensive and time-consuming, while lower sensitivity and specificity and discordance with molecular analysis limit the utility of IHC. The purpose of this study was to assess the diagnostic utility of RNA-ISH for detecting MDM2 overexpression in liposarcomas.
Design: MDM2, positive RNA control (PPIB) and negative RNA control (DapB) RNA-ISH (Advanced Cell Diagnostics) was performed on representative formalin-fixed paraffin-embedded whole tissue sections from retrospectively identified lipomas and DDLPS (cases from 2017) and previously constructed tissue microarrays (TMAs) containing DDLPS, WDLPS, and spindle cell lipomas (cases from 1999-2007). Cases with positive corresponding PPIB staining were manually and independently scored for MDM2 staining by two study pathologists. For whole-section cases, a single 40X field with maximal staining was scored. For TMAs, scores were averaged across all evaluable tissue cores from a given case. RNA-ISH signal intensity for individual tumor cells was scored as indicated by the manufacturer (0-4). A cumulative H-score was determined from the products of signal intensity and percentage of cells (i.e., H-score = [A% × 0] + [B% × 1] + [C% × 2] + [D% × 3] + [E% × 4]; total range = 0 to 400).
Results: MDM2 RNA-ISH scores were highly concordant between the two study pathologists for all TMA cases scored ($r = 0.983$; $P < 0.05$). Whole-section cases demonstrated high MDM2 expression by RNA-ISH in DDLPS (median = 295, range = 220-325; n = 5), with low expression in lipomas (median = 0, range = 0-20; n = 5). Only fourteen (13.6%) of 103 lipomatous tumors were able to be scored for MDM2 expression from the TMAs; the vast majority of cases failed to show corresponding PPIB staining. Regardless, high MDM2 expression was observed in DDLPS (median = 238, range = 115-326; n = 11) and WDLPS (H-score = 400, n = 1) with low expression in spindle cell lipomas (H-score < 10; n = 2).
Conclusion: RNA-ISH is useful for detecting MDM2 overexpression in DDLPS. Analysis of additional lipomatous tumors (WDLPS, pleomorphic liposarcoma, myxoid liposarcoma, etc.) and comparison to MDM2 FISH and MDM2 IHC is ongoing.

#25 - Clinical Utility and Concordance of Upper Urinary Tract Cytology and Biopsy in Predicting Clinicopathologic Features of Upper Tract Urothelial Carcinoma

Caroline T Simon, Stephanie L Skala, Martin Magers, Arul M. Chinnaiyan, Alon Weizer, Samuel Kaffenberg, Daniel Spratt, Jeffrey Montgomery, Aaron M. Udager, Madelyn Lew, Rohit Mehra

Manuscript: In preparation

Background: The diagnosis of upper tract urothelial carcinoma (UTUC) can be made on biopsy or upper tract washings. Endoscopic access to these lesions is often difficult, so pre-operative biopsy and cytology specimens are often less than ideal. However, diagnosis of large tumors or high-grade malignancy in the upper tract often results in definitive nephroureterectomy. Herein, we investigate the clinicopathologic factors contributing to the decision to resect UTUC, as well as the concordance between biopsy/cytology and resection with respect to grade and stage.
Design: UTUC cases with resections performed between 2000 and 2016 were retrospectively identified from the surgical pathology database at a single large academic institution. All cases with biopsy and/or cytology material available for review were included in this cohort of 130 patients. Biopsy, cytology, and resection materials were re-reviewed by three pathologists, and pre- and post-operative diagnoses were examined for concordance.
Results: The decision to proceed to nephroureterectomy was made based on the results of upper urinary tract biopsy (45/130, 35%), cytology (17/130, 13%), biopsy and cytology (3/120, 2.5%), biopsy and clinical (12/130), biopsy and radiologic (2/130), cytology and clinical (4/130), clinical and radiologic (3/130, 9.2%), radiologic (3/130, 2.3%), or clinical features (41/130, 31.5%). The most common clinical features noted to play a role in triggering a definitive resection were large size (35), difficult endoscopic access (9), multifocality (9), and persistence after BCG or chemotherapy (7). 107 patients had biopsies available for review. Twenty-six biopsied tumors (24%) were upgraded (14 from low-grade, 2 from suspicious for malignancy, 10 from non-neoplastic) to high-grade (noninvasive or invasive) at the time of resection, whereas 3 biopsied tumors (2%) were downgraded on resection. In 34 cases (32%), invasion was identified only at the time of resection. 13 cases (10%) had divergent features identified only on definitive resection; 1 case (0.8%) had divergent features identified on biopsy only. Twenty-nine cases without positive pre-operative cytology (45%, n=64) demonstrated high-grade UTUC on resection. Five cases had suspicious cytology, 11 atypical, and 13 negative. Of the 17 UTUC with low-grade histology on resection, 8 (47%) demonstrated abnormal cytology, including 2 cases called positive. A total of six patients were non diagnostic with one patient having a negative biopsy and negative cytology and five patients with a negative biopsy and no cytology performed.
Conclusion: Although the decision to proceed to nephroureterectomy for treatment of UTUC is often based on biopsy and/or cytology specimens, a large subset of UTUC are upgraded and upstaged at the time of resection.

#26 - Morphologic Comparison of SMARCB1 (INI-1)-Deficient Sinonasal Carcinoma and Sinonasal Undifferentiated Carcinoma Nominates Mitotic-Apoptotic Index as a Potential Diagnostic Discriminator

Steven C. Weindorf, Jonathan B. McHugh, Aaron M. Udager

Presented at: Accepted for presentation at USCAP 2018
Manuscript: In preparation

Background: SMARCB1 (INI-1)-deficient sinonasal carcinoma is a recently described diagnostic entity in head and neck pathology that may show overlapping morphologic and/or clinical features with other poorly-differentiated or small round cell tumors of the sinonasal tract, including sinonasal undifferentiated carcinoma (SNUC). To date, no definitive morphologic differences have been described that reliably distinguish SMARCB1 (INI-1)-deficient sinonasal carcinoma from SNUC without the use of ancillary studies [i.e., INI-1 immunohistochemistry (IHC)]. Therefore, we sought to explore potential diagnostic clues to the diagnosis of SMARCB1 (INI-1)-deficient sinonasal carcinoma.
Design: All undifferentiated sinonasal carcinomas at a single large academic institution between June 2013 and June 2017 were retrospectively identified. Blinded to the specific diagnosis, available H&E slides were reviewed concurrently by two study pathologists to assess morphologic features, including cytoplasm, nuclei, nucleoli, chromatin, and architecture; in addition, the presence and qualitative extent of cytologic pleomorphism and rhabdoid features was recorded. Counts of mitotic and apoptotic figures in ten high-power (40X) fields were performed independently by two study pathologists and averaged. INI-1 IHC was subsequently performed by the clinical IHC laboratory on sectioned tissue from all tumors, and cases were grouped for comparison based on the presence or absence of nuclear INI-1 staining. Clinical information was manually extracted from the electronic medical record.
Results: A total of 8 undifferentiated sinonasal carcinomas were identified, of which 2 (25%) showed loss of nuclear INI-1 staining by IHC [i.e., SMARCB1 (INI)-1 sinonasal carcinoma]. Comparison of clinical information and morphologic features showed significant overlap among all cases, however, the mitotic count, apoptotic count, and mitotic-apoptotic count were relatively lower in INI-1-deficient tumors (Table 1); in addition, these INI-1-deficient tumors were more likely to show rhabdoid features and lack significant cytologic pleomorphism (Table 1).

Table 1	SNUC (n=6)	SMARCB1 (INI-1)-Deficient Sinonasal Carcinoma (n=2)
Cytologic pleomorphism	No = 2	No = 2
	Yes = 4	Yes = 0
	(Anaplasia =1)	
Rhabdoid features	None = 4	None = 0
	Focal = 1	Focal = 0
	Non-focal = 1	Non-focal = 1
	Extensive = 0	Extensive = 1
Mitotic count/10 40X fields ($\bar{x}$)	57 (range: 41-121)	26 (range: 13-38)
Apoptotic count/10 40X fields ($\bar{x}$)	60 (range: 34-139)	17 (range: 8-25)
Mitotic-apoptotic count/10 40X fields ($\bar{x}$)	111 (range: 84-260)	42 (range: 21-63)

Conclusion: Although SMARCB1 (INI-1)-deficient sinonasal carcinoma shares many clinical and morphologic features with SNUC, our preliminary data indicate that the mitotic-apoptotic index (MAI) is a potential diagnostic discriminator. If this finding is confirmed in larger studies, MAI assessment may allow for more judicious use of INI-1 IHC in the work-up of undifferentiated sinonasal carcinomas.

.

#27 - A Single-Page Web Application Based Dashboard for Sebia Capillary Electrophoresis

Keluo Yao, Christopher Sobeck, Christopher Williams, Stephen Fayz, Forrest Huls, Sean Li, Lee Schroeder, David Keren, David McClintock, Ulysses Balis

Manuscript: In preparation

Background: The Sebia Capillarys (Sebia, Issy-les-Moulineaux, France) software provides limited user interface, functionally, and portability to adequately manage the serum protein electrophoresis assay results produced by the Sebia instruments. Routine workflow requires manual entry of laboratory data and physical onsite interpretation. The availability of bidirectional data flow through web API interface of electronic medical record (EMR) and the recent Single-Page Application (SPA) paradigm has given us the technologies to potentially overcome these limitations. This study investigates the feasibility of building a "dashboard" for Sebia capillary electrophoresis interpretation using these technologies..
Design: We designed SPA wireframe based on these principles: 1) automated complete laboratory data request from the EMR (Epic); 2) modern and interactive user interface, laboratory data, and serum protein electrophoresis schematics; 3) secure, flexible, and portable user access.
Results: Figure 1 shows the overall SPA wireframe design of the demonstration dashboard software. The dashboard's functionalities depend on two main components: 1) application programming interface (API) server and 2) user interface (UI) server. The API server runs server sided scrips to request laboratory data from Epic via the representational state transfer (REST) API with secure authentication. The UI server provides a graphical user interface and dynamically generated content and allows: 1) text field for entering patient identification information for the API server to request clinical data; 2) display of relevant laboratory data (eg, total albumin level) and relevant interfering medications (eg, radio contrast agents); 3) display of serum protein electrophoresis schematics using D3.js v4 library. The overall UI server architecture is built using Node.js v8, architecture to allow server sided script execution and is optimized for future expandability and maintenance by using webpack "code on demand" and riot.js v3. Security is achieved through virtual private network access.
Conclusion: We have built a working demo that proves the feasibility of a dashboard software that fulfills the design requirements. The next steps of this project include the full development/optimization of the UI server to allow testing and implementation.

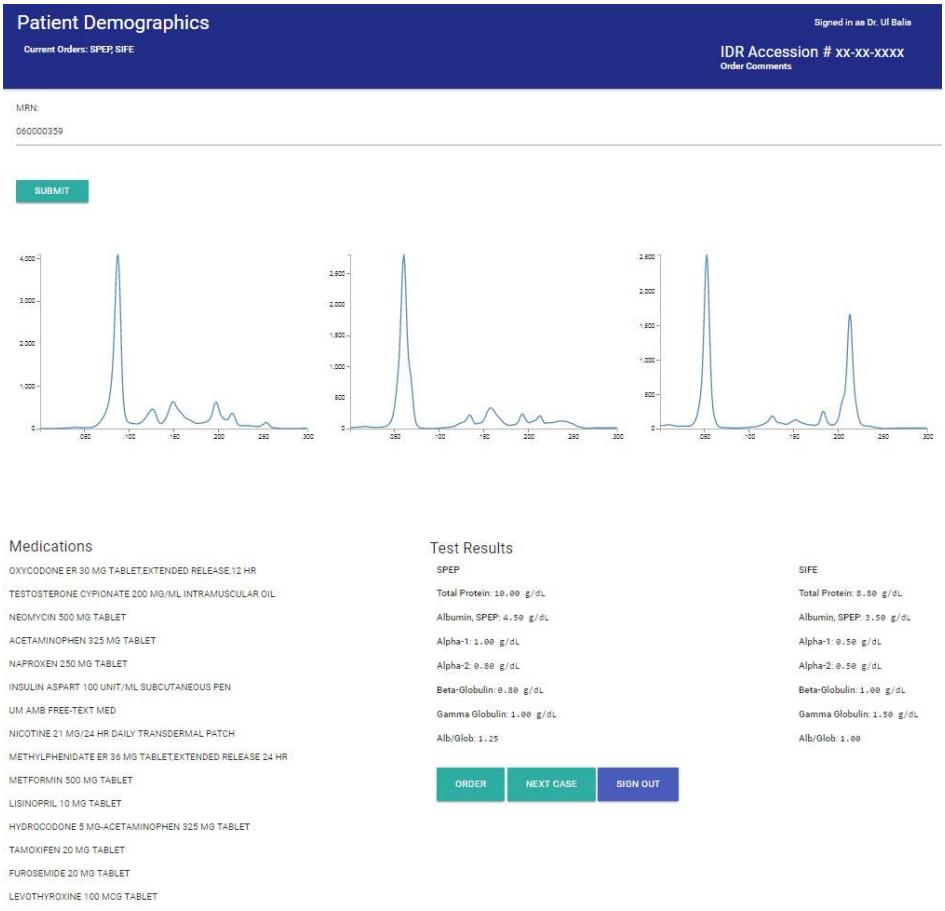

Figure 1: Overall wireframe design of the Sebia capillary electrophoresis dashboard

#28 - Retrospective Analysis of Follicular Neoplasm Cytomorphology Using a Robust and Semi-automated Digital Image Algorithm

Keluo Yao, Xin Jing, Amer Heider, Judy C Pang, Robertson Davenport, Madelyn Lew

Manuscript: In preparation

Background: Identification of follicular neoplasms based on cytologic features in preoperative thyroid fine needle aspirations (T-FNA) alone is subject to significant uncertainty and can lead to unnecessary surgeries. Frequently T-FNA are evaluated in liquid-based preparations (LBP), which allow for optimal visualization of nuclear cytomorphology and digital image analysis (DIA) applications. This study investigates the feasibility of utilizing DIA to identify characteristics that may increase accuracy in the detection of follicular neoplasms on LBPs from T-FNA.
Design: From the electronic medical database, 10 T-FNAs diagnosed as follicular lesions of undetermined significance (FLUS) with subsequent diagnoses of follicular adenoma on surgical resections and 10 T-FNAs diagnosed as benign with concordant surgical resections were identified for evaluation. Digital images of 10 randomized mid-power (10x) and high-power (40x) fields on LBP were obtained using a DP71 camera (Olympus, USA) on an Olympus BX51 microscope with CellSens Entry v1.12 (Olympus, USA). 40x fields were analyzed for nuclear features of follicular cells while 10x fields were analyzed for overall specimen cellularity (Table 1). ImageJ v1.51p (NIH, USA) was used for image processing/analysis.
Results: Optimal automatic segmentation consists of image pre-processing with background subtraction, followed by color deconvolution of blue channel in grey scale format (Figure 1). The automatic threshold is then applied which results in robust extraction of cell nuclei, which are then analyzed as particles to determine quantitative and qualitative features (Table 1). Cutoffs (Table 1) were set to filter out background cells (eg, neutrophils) and other artifacts (eg, fibrin). The cellularity data on 10X fields was extracted similarly and determined by average total nuclei area per field.
Conclusion: In our preliminary data, we have successfully designed a robust semi-automated DIA algorithm using open source software that identified visually challenging/subjective features such as specimen cellularity and average follicular nuclear size that may improve accuracy in identification of follicular neoplasms on T-FNA on LBP cytologic material. Next steps of our study include increasing the number of evaluated cases to further delineate features that can improve accuracy in diagnosis follicular neoplasms on T-FNAs, developing techniques to provide predictive power, validate reproducibility, and applying our algorithm to other thyroid lesions.

Table 1: Cytomorphology Features Examined By the Semi-automated Digital Image Algorithm

	Follicular Adenoma T-FNA	Benign T-FNA	p value
Cellularity (% of area)	1.50 ±1.12%	0.96 ± 1.30%	0.0061
Average follicular cell nuclear size	612 ± 89 pixels[1]	538 ± 109 pixels	0.000026
Circularity[2]	0.72 ± 0.05	0.74 ± 0.05	0.02
Mean grey level[3]	210 ± 6	205 ± 9	0.21
Cutoffs for 40X cell/particle analysis			
Particle size filter	200 to 1200 pixels		
Circularity filter	0.5 to 1.0		

[1] Each pixel represents an area of approximately 0.1µm2
[2] Based on the formula: $\frac{4\pi \times [\text{Area}]}{[\text{Perimeter}]^2}$
[3] Average pixel values of the nuclear chromatin (blue channel)

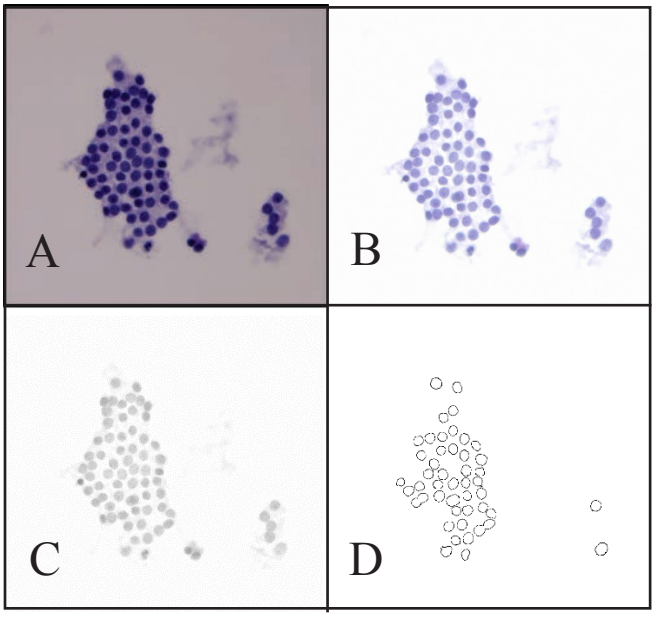

Figure 1: The segmentation and feature extraction of follicular cells starts with the original image (A), followed by the background subtraction (B), conversion to 8-bit grey scale image from the blue channel (C), and finally automatic threshold segmentation and nuclear feature extraction (D).

#29 - Targeted Genomic Profiling Reveals Highly Recurrent Molecular Alterations in the Malignant Progression of Sinonasal Papilloma to Sinonasal Squamous Cell Carcinoma, including *CDKN2A* Mutation/Deletion and *TP53* Mutation

Osman H. Yilmaz, Komal R. Kunder, Jonathan B. McHugh, Bryan L. Betz, Scott A. Tomlins, Noah A. Brown, Aaron M. Udager

Presented at: Accepted for presentation at USCAP 2018
Funded by: AP Project Funding Committee
Manuscript: In preparation

Background: Inverted sinonasal papilloma (ISP) and oncocytic sinonasal papilloma (OSP) are benign tumors that may be associated with sinonasal squamous cell carcinoma (SNSCC). Our group recently identified frequent somatic *EGFR* mutations in ISP and *KRAS* mutations in OSP and demonstrated concordant mutations in associated SNSCC components, confirming a clonal relationship between these tumors. In the present study, we utilize targeted next-generation DNA sequencing (DNAseq) to characterize the landscape of molecular alterations involved in malignant progression from papilloma to SNSCC.
Design: ISP-SNSCC (*n* = 18) and OSP-SNSCC (*n* = 2) at a single large academic institution were retrospectively identified from previously published tumor cohorts. Representative formalin-fixed paraffin-embedded tissue was selected for targeted DNAseq using the Oncomine Comprehensive Assay and an Ion Torrent Proton sequencer; when available, tissue from the corresponding papilloma component was also selected. Somatic variants and copy number alterations (CNA) were identified via in-house bioinformatics pipelines, and prioritized alterations were nominated by manual curation using previously established criteria.
Results: ISP-SNSCC demonstrated a total of 70 prioritized somatic variants (median per tumor = 3; range = 1-12). All tumors harbored *EGFR* mutations, including a previously unreported exon 6 hotspot variant; other recurrently mutated genes included *TP53* (*n* = 13), *CDKN2A* (*n* = 8), *NFE2L2* (*n* = 4), *PIK3CA* (*n* = 3), *FBXW7* (*n* = 3), and *NOTCH1* (*n* = 3). A total of 36 CNA were identified in ISP-SNSCC (median per tumor = 1.5; range = 0-5). *CDKN2A* (loss; *n* = 8) was the most frequent CNA, with 6 tumors showing two-copy loss ("deep deletion") and 2 showing single-copy loss; other recurrent CNA include *TERT* (gain; *n* = 5) and *SOX2* (gain; *n* = 3). All ISP-SNSCC harbored at least one *TP53* or *CDKN2A* alteration, with >85% of tumors having at least one *CDKN2A* alteration; all 7 matched ISP were negative for *TP53*/*CDKN2A* mutations and showed no CNA. Both OSP-SNSCC demonstrated *KRAS* G12D mutations with concurrent *TP53* mutations. *EGFR* was amplified in two ISP-SNSCC, and *KRAS* was amplified in one OSP-SNSCC.
Conclusion: Malignant progression of sinonasal papilloma to SNSCC involves highly recurrent molecular alterations, including *TP53* mutation and *CDKN2A* mutation/deletion. Common molecular alterations in head and neck squamous cell carcinoma also occur in subsets of sinonasal papilloma-associated SNSCC.

#30 - High Rate of FISH False Negative Results in the Detection of Homozygous Loss of CDKN2A in Difficult Melanocytic Tumors

Nicholas Zoumberos, Kenneth Yu, Min Wang, Paul Harms, May Chan, Rajiv Patel, Lori Lowe, Douglas Fullen, Aleodor Andea

Presented at: Will be presented at USCAP 2018
Manuscript: In preparation

Background: Although histologic interpretation remains the gold standard for the diagnosis of melanoma, molecular methods based on the detection of copy number changes by single nucleotide polymorphism (SNP) microarrays or fluorescence in-situ hybridization (FISH) are increasingly being used in the diagnosis of histologically ambiguous lesions. One of the most significant markers of melanoma is homozygous deletion of the *CDKN2A* gene, which encodes p16. Detection of this abnormality by FISH is considered to correlate with increased risk for adverse outcome and is often used to favor a diagnosis of melanoma.
Design: From our SNP array database of 263 melanocytic tumors we identified 32 cases with homozygous loss of *CDKN2A.* FISH with a commercially available 9p21 probe for *CDKN2A* was performed in 14 cases with available material and compared with the SNP array results. For the remaining 18 cases, the results of FISH testing were predicted based on the location of the 9p21 probe relative to the area of homozygous deletion.
Results: The typical pattern on SNP array consisted of deletion of a large portion of 9p or entire chromosome 9 on one allele combined with a smaller deletion of the other allele overlapping the *CDKN2A* gene. The average size of the area of homozygous deletion was 2.6 MB (range 0.02-13.75 MB). FISH detected homozygous deletions of 9p21 in only 8/14 cases (57%). The average size of deletion in cases with false negative FISH was smaller than in cases with positive FISH: 0.22 MB (range 0.02-0.6 MB) versus 4.26 MB (range 0.25-13.75 MB) respectively. Failure to detect the homozygous *CDKN2A* deletion was associated with lack of complete overlap between the FISH probe (designed with a larger overhang towards the p-terminus) and an area of homozygous deletion that was small or extended only towards the centromere. For the 18 cases without FISH, the location of the probe relative to area of deletion predicted detection of homozygous loss in 14 cases (61%).
Conclusion: We report a relatively high rate of false negative FISH results (41%) for detection of homozygous loss of *CDKN2A* gene compared to SNP array, especially when the deleted area is small (<0.6 MB) or asymmetrically located. This represents a significant diagnostic pitfall when using FISH in the diagnosis of difficult melanocytic tumors.

Keynote Speaker:

Pedram Argani, MD
Director and Principal Consultant
Breast Pathology Service
Professor of Pathology
Johns Hopkins University School of Medicine

" MiT Family Translocation Carcinoma of the Kidney"

Dr. Pedram Argani is a professor of pathology at the Johns Hopkins University School of Medicine. His area of clinical expertise is breast pathology, where he reviews approximately 1,000 breast consultation cases each year. He is internationally recognized as an expert anatomic pathologist.

Dr. Argani serves as the director and principal consultant of the Breast Pathology Service in the Sidney Kimmel Comprehensive Cancer Center.

He received his undergraduate degree from Princeton University. He earned his M.D. from University of Pennsylvania Health System School of Medicine where he also completed his residency in anatomic pathology. Dr. Argani performed a fellowship in oncologic and molecular pathology at Memorial Sloan-Kettering Cancer Center.

Dr. Argani is a member of the steering committee of the Breast Center at Johns Hopkins. He is on the editorial board of numerous scientific journals, including the American Journal of Surgical Pathology, the American Journal of Clinical Pathology, Modern Pathology, and the International Journal of Surgical Pathology. Dr. Argani won the Arthur Purdy Stout Prize from the United States and Canadian Academy of Pathology for his contributions to the advancement of diagnostic pathology. In addition, he was awarded the Professors' Award for Excellence in Teaching at Johns Hopkins University School of Medicine.

Notes

Notes

Notes

Notes

Notes